Supporting Information

Characterisation, degradation and regeneration of luminescent Ag_{29} clusters in solution

Marte van der Linden,[a,b] Arjan Barendregt,[c,d] Arnoldus J. van Bunningen,[e] Patrick T. K. Chin,[e] Dominique Thies-Weesie,[f] Frank M. F. de Groot[a] and Andries Meijerink[e]

[a] *Inorganic Chemistry & Catalysis, Debye Institute for Nanomaterials Science, Universiteit Utrecht, Universiteitsweg 99, 3584 CG Utrecht, the Netherlands. E-mail: M.vanderLinden1@uu.nl*
[b] *ID26, European Synchrotron Radiation Facility (ESRF), 71 Avenue des Martyrs, 38000 Grenoble, France*
[c] *Biomolecular Mass Spectrometry and Proteomics, Utrecht Institute for Pharmaceutical Sciences and Bijvoet Centre for Biomolecular Research, Universiteit Utrecht, Padualaan 8, 3584 CH Utrecht, the Netherlands.*
[d] *Netherlands Proteomics Center, Padualaan 8, 3584 CH, Utrecht, The Netherlands.*
[e] *Condensed Matter & Interfaces, Debye Institute for Nanomaterials Science, Universiteit Utrecht, Princetonplein 5, 3584 CC Utrecht, the Netherlands.*
[f] *Van 't Hoff Laboratory for Physical and Colloid Chemistry, Debye Institute for Nanomaterials Science, Universiteit Utrecht, Padualaan 8, 3584 CH, Utrecht, the Netherlands.*

Contents

S1 Synthesis and optical properties of Ag clusters

19 mg lipoic acid (92 µmol) and 7 mg $NaBH_4$ (0.19 mmol) were placed in a 40 or 20 mL glass vial with 14 mL water. This was stirred (using a magnetic stirring bean) until all LA had dissolved. Next, 700 µL 25 mM $AgNO_3$ (17.5 µmol) was added (the solution turned turbid), followed by 10 mg $NaBH_4$ (0.26 mmol) in 2 mL water. The vial was wrapped in aluminium foil to minimise the exposure of the clusters to light. After $3-5$ hours, the clusters had formed. The synthesis was performed at room temperature and magnetic stirring was continued throughout. Samples were stored in the dark at room temperature.

When synthesising clusters with different Ag:LA ratios, the amount of $AgNO_3$ was kept the same while the amounts of LA and $NaBH_4$ in the first step were changed. Maximum emission intensity as a function of LA concentration and normalised emission spectra of Ag clusters with Ag:LA =1:5.3 (standard ratio) and 1:0.6 are given in Fig. S1. As can be seen, with low LA concentration the shape of the emission peak varies from sample to sample (see also Fig. S34).

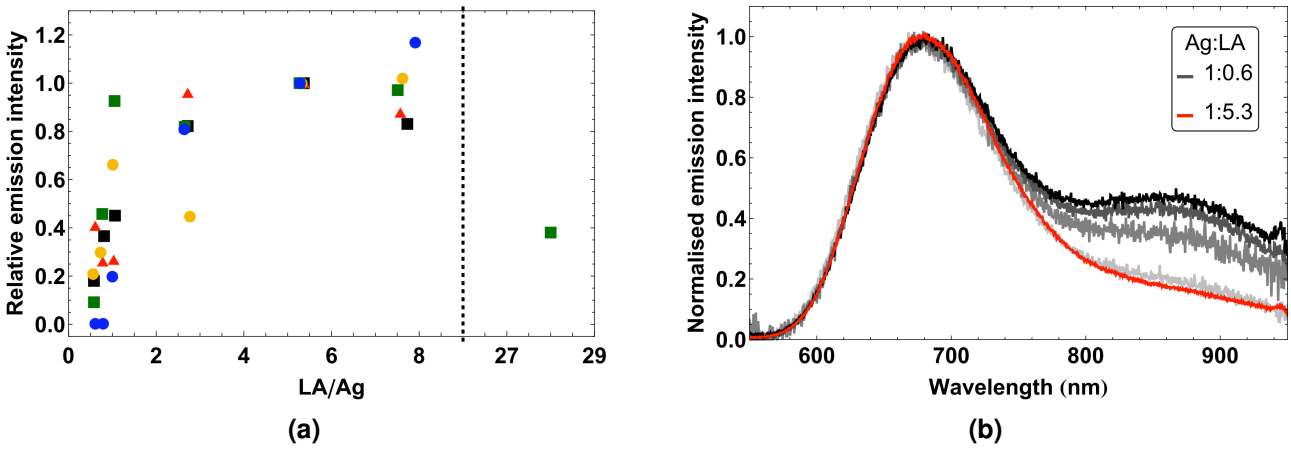

Figure S1 a) Maximum emission intensity for samples with various Ag:LA ratios, relative to samples with Ag:LA = 1:5.3. An excess of ligands is required in order to observe high luminescence intensity. Different colours represent samples prepared on different days. b) Normalised emission spectra of different samples with low ligand concentration (Ag:LA = 1:0.6, in grey and black) and a standard sample (Ag:LA = 1:5.3, in red). Samples with low ligand concentrations have higher relative emission intensity in the near-infrared (NIR), but differences in shape of the emission peak suggests the synthesis of these clusters is not very reproducible.

Clusters were synthesised in the presence of existing Ag_{29} to investigate whether they would behave as classical seeds for the formation of larger nanoparticles. A synthesis of Ag clusters was done on $\frac{1}{2}$scale. Just before addition of $AgNO_3$ and $NaBH_4$ solutions, half of a previously prepared sample was added to it. The seeded sample was identical to normal samples in all respects (total volume and concentration of reagents). UV-Vis spectra of the finished seeded sample and a standard sample prepared on the same day are virtually indistinguishable (Fig. S2).

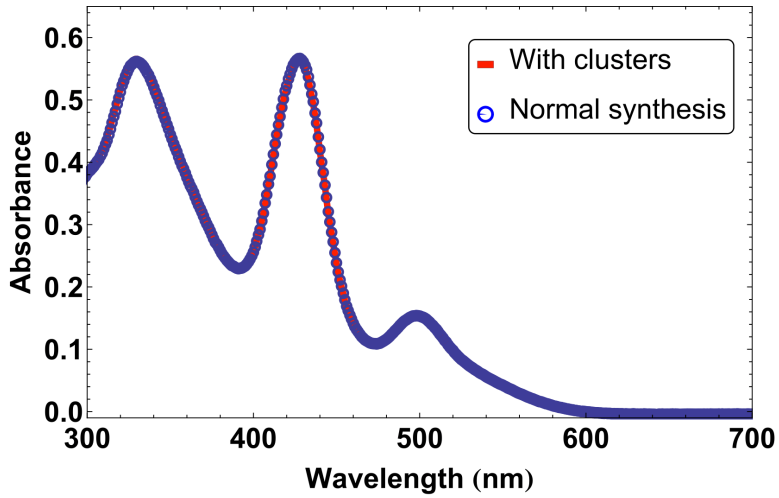

Figure S2 UV-Vis spectra of a batch of clusters synthesised in the presence of existing clusters (red) and a normal batch of clusters (blue). Samples have been diluted 6x with water.

S2 Analytical ultracentrifugation (AUC)

S2.1 Sedimentation velocity analytical ultracentrifugation (SV-AUC)

After centrifugation at 60.000 rpm, the Ag clusters have sedimented and absorption spectra were recorded in the top of the AUC cell (Fig. S3a, r = 6.2 cm) to identify the small species with sedimentation coefficient close to 0 S. Absorption spectra of LA, LA + $AgNO_3$ and DHLA + $AgNO_3$ are given in Fig. S3b. DHLA, dihydrolipoic acid, is the reduced form of LA (two thiol groups instead of a disulfide bond), obtained by reaction of LA with $NaBH_4$. Clearly, the small species observed in SV-AUC correspond to free LA, and not to small Ag-LA complexes.

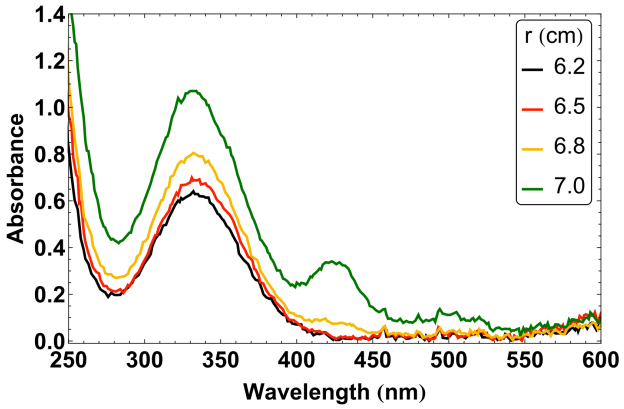

(a) Absorption spectra at various positions in the AUC cell, after centrifugation at 60.000 rpm. The Ag clusters have sedimented, so these absorption spectra are of the light species with sedimentation coefficient close to 0 S. r is the radial position, where r = 6.2 cm is close to the meniscus. At r = 7.0 cm (green) there is also some absorption at 425 and 500 nm, indicating the presence of clusters close to the bottom of the cell. The pathlength of the cells for absorption is 1.2 cm.

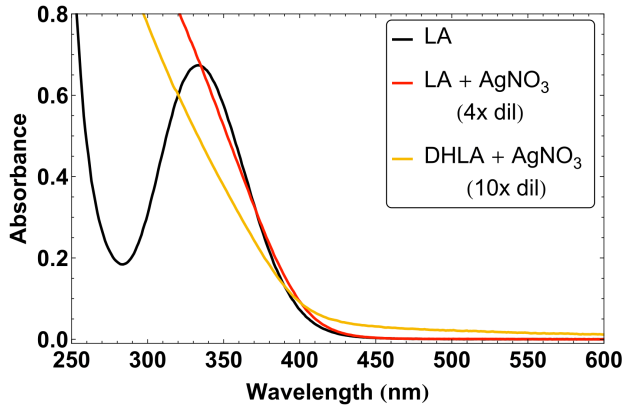

(b) Absorption spectra of LA (black), LA with $AgNO_3$ (red) and reduced LA with $AgNO_3$ (yellow). The strong absorption feature at 333 nm is only visible for LA. The dilution is relative to the concentrations in the cluster samples.

Figure S3

S2.2 Sedimentation equilibrium analytical ultracentrifugation (SE-AUC)

We performed sedimentation equilibrium measurements of undiluted, 2x and 4x diluted Ag clusters solution at three different speeds (23.000, 35.000 and 43.000 rpm) at 423, 485 and 528 nm. For undiluted samples, the data could be fitted to a single species model with one component. This species was found to have a molar mass of 6.6 kDa. For 2x and 4x diluted samples, a model with two components was used. One species was the same as for the undiluted sample, with a molar mass of 6.6–6.7 kDa. The second species was found to have a molar mass of 15.2 kDa or 26.0 kDa for 2x and 4x diluted, respectively. It appears that these heavy species are formed during the measurement. To check if dilution affects the stability of the clusters, we prepared a 4x diluted sample and measured the UV-Vis absorption spectrum every day for a week (the same timescale as for SE-AUC experiments). During this time, the absorption peaks became weaker (see Fig. S4), which is expected as cluster aggregation results in a decrease of the Ag_{29} concentration.

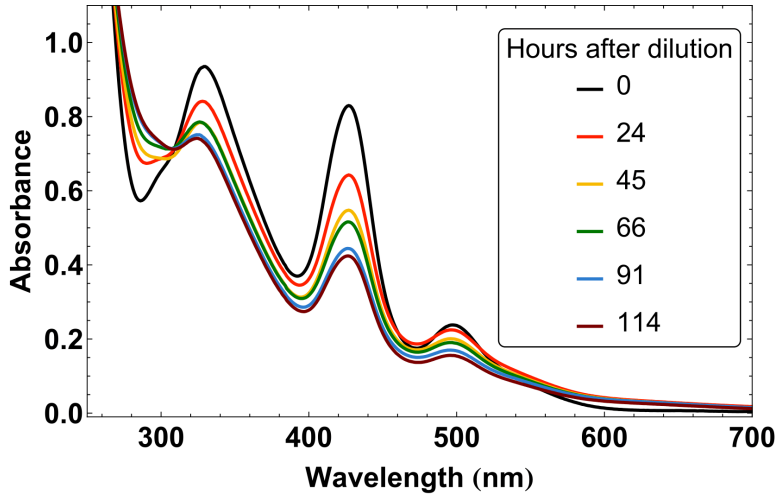

Figure S4 Absorption spectra of Ag clusters at various times after dilution (4x). The absorption peaks gradually disappear, which indicates aggregation (see also Fig. 4).

S3 Mass spectrometry

S3.1 Purification with BuOH

Purification of clusters with BuOH was done by mixing 300 µL clusters, 400 µL BuOH and 100 µL methanol in an Eppendorf vial. The vial was briefly centrifuged to speed up phase separation, and the upper colourless organic layer was removed. Next, 300 µL BuOH was added, the vial was shaken and centrifuged, and the organic layer was again removed. This was repeated until the clusters had just sedimented. Typically, 3-5 extractions with BuOH were needed. After removing the final organic layer and washing with methanol (50–100 µL), the clusters were redispersed in water (50–100 µL).

This purification method could easily be scaled up (we used up to 12 mL clusters solution) which allowed for characterisation of the purified clusters with optical spectroscopy. The amount of water for cluster redispersion was chosen so that the absorbance of as-synthesised and purified clusters was similar.

A typical mass spectrum is shown in Fig. S5. The mass difference between adjacent ion signals in each group is 22 Da which corresponds to the addition of Na^+ replacing H^+. Groups of ion signals around $m/z = 1040$ and 1080 are assigned to $Ag_{27}(LA)_{11}$ and $Ag_{29}(LA)_{11}$, respectively.

The experimental spectrum in the $z = 5-$ charge state has been compared to theoretical spectra of $[Ag_{29}(LA)_{12}]$ and $[Ag_{25}(LA)_{14}]$, the two alternative cluster compositions, in Fig. S6. As the question

of whether the $[Ag_{29}(LA)_{12}]$ cluster core is neutral or carries a $3-$ charge is arguably one of the most important, we also show the theoretical spectra for the two compositions compared to the deconvoluted spectrum (Fig. S7). Our spectra demonstrate that any contribution of species with a neutral core is minor, while the cluster with $3-$ core charge is the main species.

We also calculated theoretical mass spectra of other clusters with approximate mass of 5.6 kDa in the overall 5- charge state, with compositions between $Ag_{11}(LA)_{21}$ and $Ag_{23}(LA)_{15}$, and between $Ag_{31}(LA)_{11}$ and $Ag_{37}(LA)_{8}$ (so bigger and smaller than those already discussed). Spectra where calculated with and without core charges, for all possible H^+/Na^+ exchanges and for clusters with either all LA ligands or all HLA ligands (HLA is assumed to have one $-SH$ group thus making it 1 Da heavier than LA). None of these other clusters have mass spectra that satisfactorily explain our data. In each case, there were unexplained ion signals (or missing ion signals) and/or a large shift between experimental and theoretical spectra.

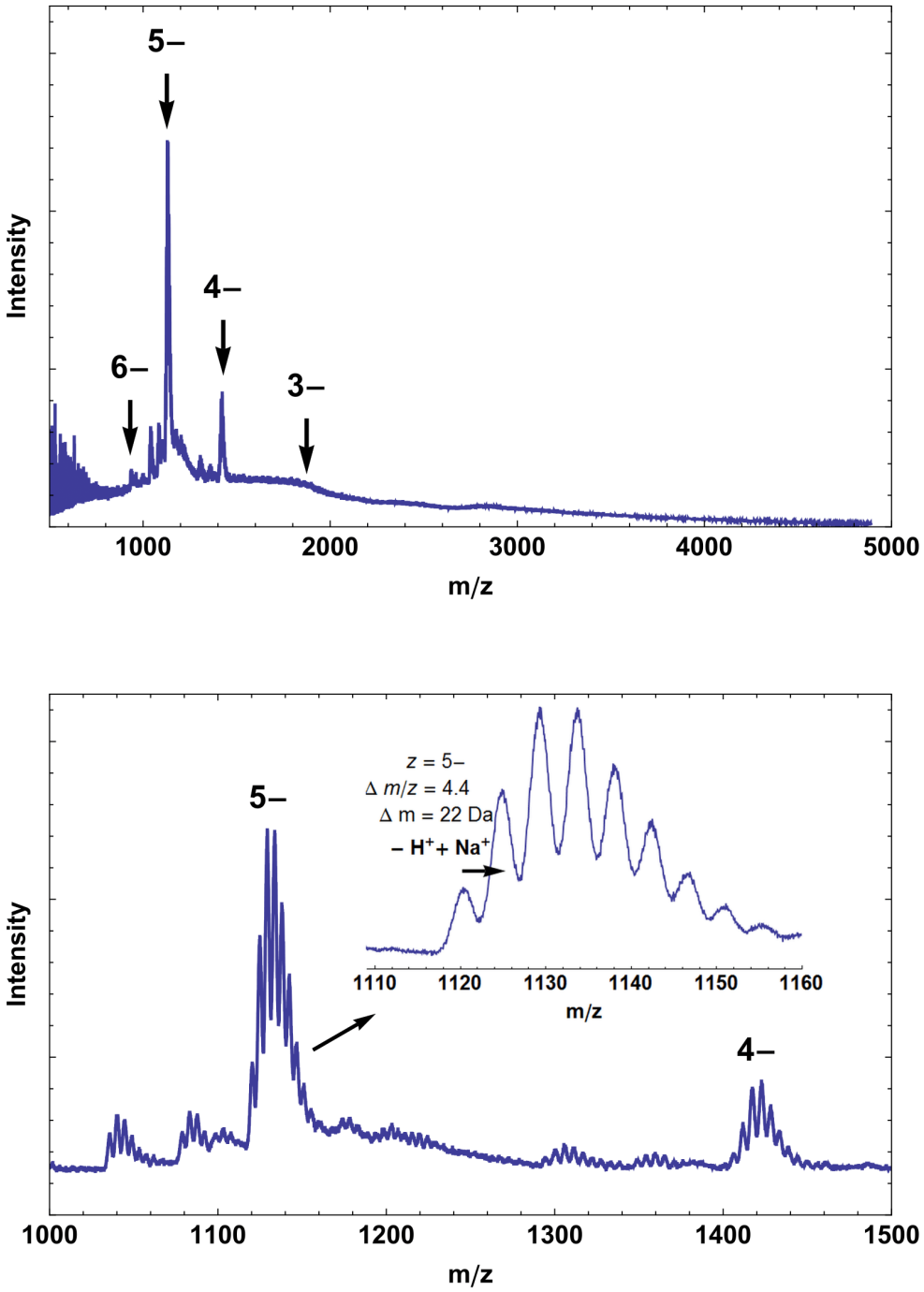

Figure S5 ESI-MS spectrum (sample cone voltage, SCV = 7 V) of Ag clusters purified with BuOH. The most intense signal is from a $z = 5-$ species with mass 5.6 kDa. This cluster also exists in other charge states. The $z = 6-$, $4-$ and $3-$ species (around $m/z = 930$, 1400 and 1870) are marked. A weak feature around $m/z = 2800$ could be the cluster in $z = 2-$ charge state, formed by association of a cation (H^+ or Na^+) to the cluster. The bottom image shows the $z = 5-$ and $z = 4-$ species, with a zoom in of the $z = 5-$ species in the inset so that the individual ion signals due to H^+/Na^+ exchange can be clearly seen.

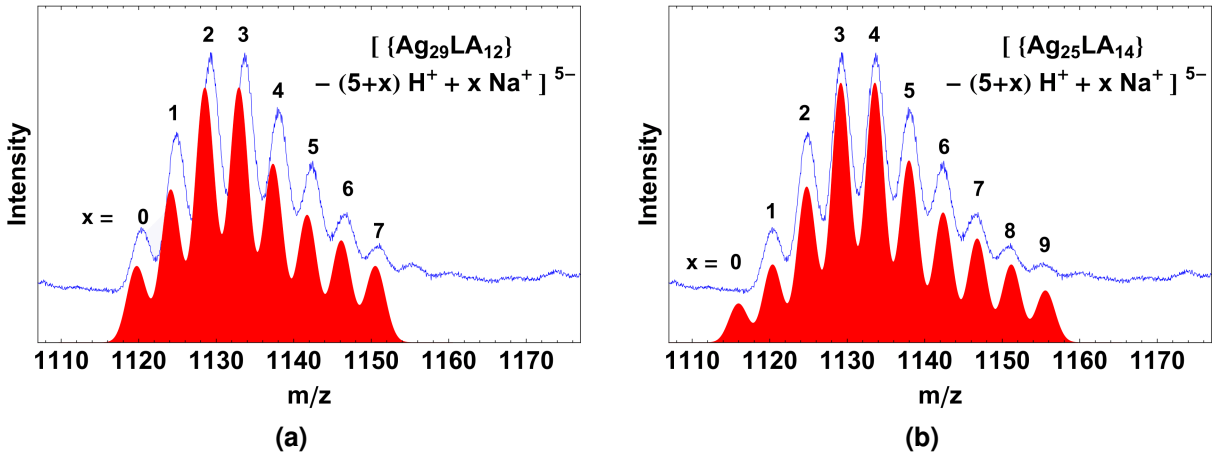

Figure S6 Experimental mass spectrum (blue) and theoretical mass spectrum (red) for two other proposed cluster compositions. a) $[Ag_{29}(LA)_{12} - (5+x)H^+ + xNa^+]^{5-}$, with neutral core charge, experimentally observed by Russier-Antoine et al.[1] b) $[Ag_{25}(LA)_{14} - (5+x)H^+ + xNa^+]^{5-}$, with neutral core charge, the composition proposed in our previous article.[2] The theoretical spectra are shown for all possible x, where x is the number of H^+/Na^+ exchanges. The agreement between theoretical and experimental spectrum is worse for these two clusters than for $[Ag_{29}(LA)_{12}]^{3-}$ (see Fig. 3 in main article). For a), not only is there a slight shift between the theoretical and experimental spectrum, but the ion signal at $m/z = 1155.5$ (and possibly 1160) cannot be satisfactorily explained. The mass difference between the neutral and $3-$ charged core Ag_{29} clusters is $3\,\mathrm{Da}$, which for the overall $z = 5-$ charge state is a difference in m/z of 0.6. The resolution of our mass spectrometer (2800) is sufficiently high to resolve this. For b), the most noticeable difference between theoretical and experimental spectra is the absence of the $m/z = 1116$ signal.

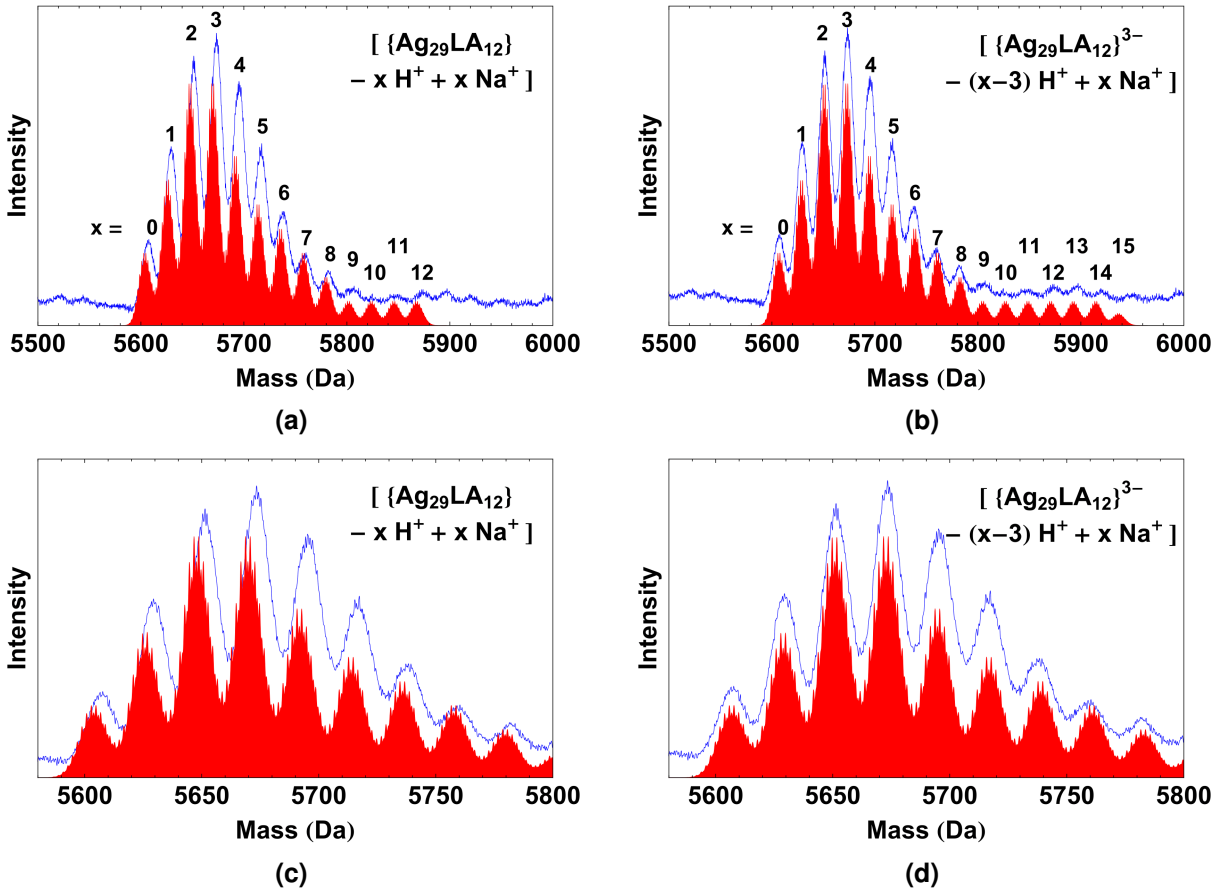

Figure S7 Deconvoluted mass spectrum (blue) and theoretical mass spectrum (red) for the two proposed cluster compositions. Spectra were deconvoluted from the $z = 6-$, $5-$ and $4-$ overall charged species to obtain spectra of the neutral species (the $3-$ overall charge state was not used as the intensity was very low). a) $[Ag_{29}(LA)_{12} - xH^+ + xNa^+]$ (neutral core, experimentally observed by Russier-Antoine et al.[1]). b) $[\{Ag_{29}(LA)_{12}\}^{3-} - (x\text{-}3)H^+ + xNa^+]$ ($3-$ charged core, the composition we propose). Note that to obtain a neutral species for the cluster with $3-$ core, $3\,H^+$ must be added to it. c) and d) show the most intense ion signals in more detail. Agreement with the deconvoluted spectrum is better for the $3-$ charged core.

Mass spectra showing signs of poly- or bidispersity are given in Fig. S8. The observed polydispersity is to some degree caused by degradation of clusters in the capillary needle during a measurement. As shown in Fig. S9, the relatively intensity of the cluster ion signal decreases during the measurements.

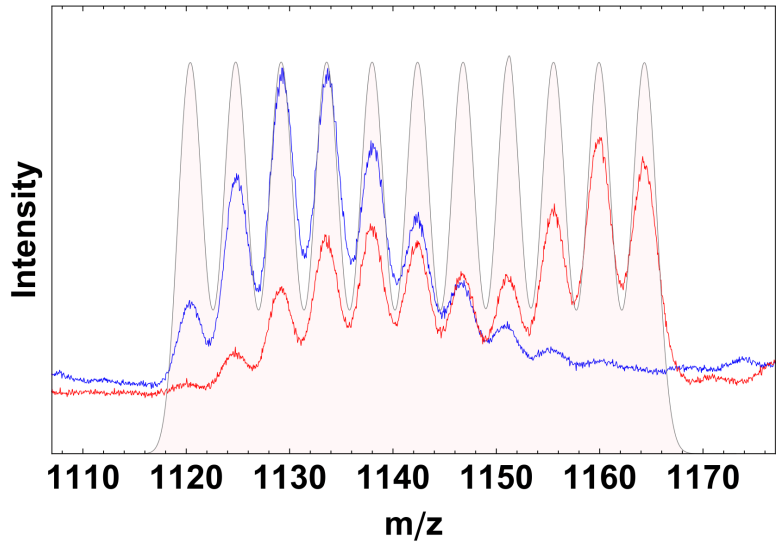

Figure S8 Red: Mass spectrum of Ag clusters purified with BuOH on a large scale, showing what appears to be two distributions of H^+/Na^+ exchange. Blue: mass spectrum from main article, shown for comparison. Also shown is the theoretical mass spectrum of $[\{Ag_{29}(LA)_{12}\}^{3-} - (2+x)H^+ + xNa^+]^{5-}$ for all x (filled graph), from the same calculation as in the main article but without scaling of ion signals with different x. It is clear that all ion signals in both experimental spectra can originate from the Ag_{29} species.

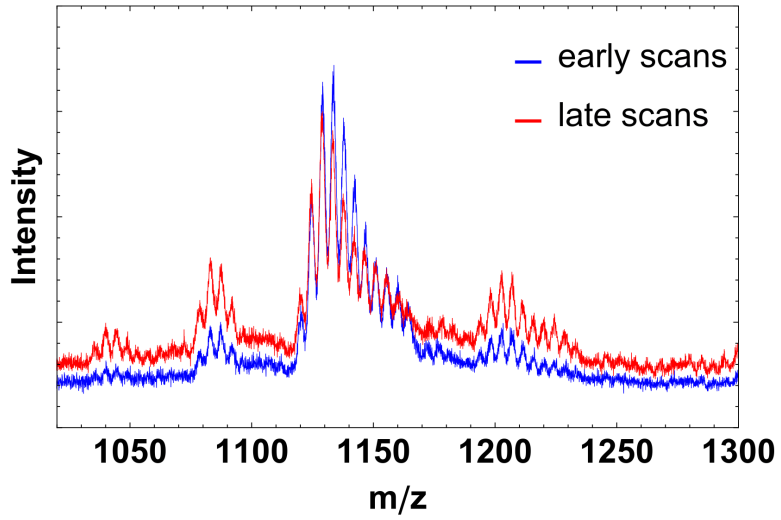

Figure S9 Blue: 20 scans early during the measurement, red: 20 scans late during the measurement. The relative intensity of the Ag_{29} signal ($m/z = 1120-1150$) decreases.

S3.2 Purification with cut-off filters

Mass spectra were recorded of clusters purified using 3 kDa cut-off filters to remove excess salts and ligands from the as-synthesised clusters solution. After initial filtration, the samples were washed twice with Milli-Q water. Mass spectra were recorded after every purification step. This purification method yields more ion signals than the BuOH purification (Fig. S10). It is possible that the cut-off filter method causes aggregation and/or fragmentation of the clusters (Fig. S11).

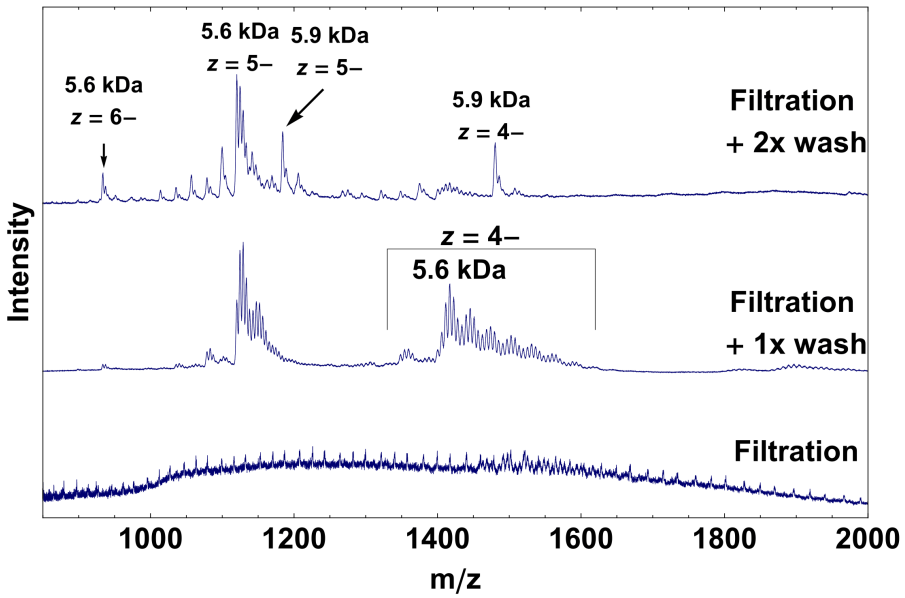

Figure S10 Mass spectra of clusters purified with cut-off filters. After initial filtration (bottom), only a broad signal is visible. After washing once with Milli-Q water (middle), many heavier species are present (up to $6.4\,\mathrm{kDa}$). After washing twice (top), the $5.6\,\mathrm{kDa}$ species dominates but there is also a significant amount of a $5.9\,\mathrm{kDa}$ species. The first ion signal in the $z = 5-$ group of the $5.6\,\mathrm{kDa}$ species, at $m/z = 1120$, dominates. This is the $[Ag_{29}LA_{12}]^{3-}$ cluster with $x = 0$ H^+/Na^+ exchanges and is consistent with the washing away of excess salts.

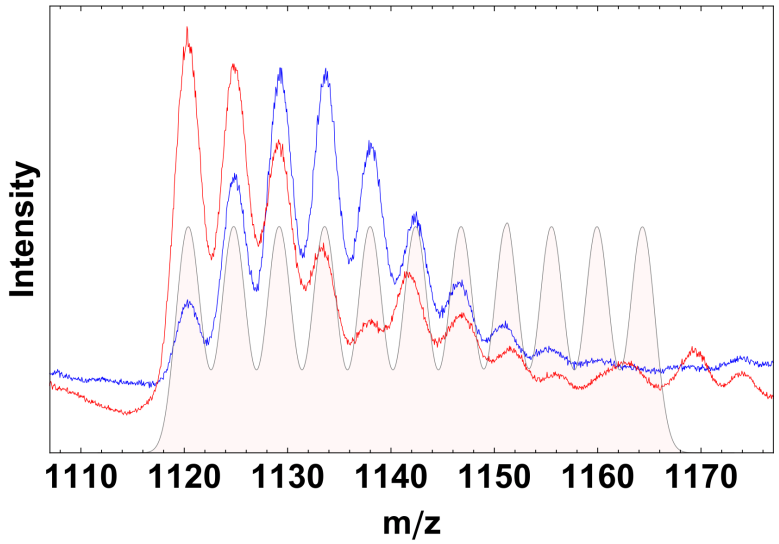

Figure S11 Red: Mass spectrum of Ag clusters purified with cutoff filters and washed twice (the same spectrum as in Fig. S10 top). Blue: mass spectrum from main article, shown for comparison. Also shown is the theoretical mass spectrum of $[\{Ag_{29}(LA)_{12}\}^{3-} - (2+x)H^+ + xNa^+]^{5-}$ for all x (filled graph), from the same calculation as in the main article but without scaling of peaks. The ion signal corresponding to $x = 0$ H^+/Na^+ ($m/z = 1120$) exchanges is the most intense for the clusters purified with filters due to removal of salts. Note that there appears to be a second distribution of ion signals at $m/z = 1135 - 1155$ for the red spectrum, where the agreement with the theoretical spectrum is not as good. This could be due to cluster degradation during filtration

S3.3 High SCV and tandem MS

Tandem MS spectra were recorded with $[\{Ag_{29}LA_{12}\}^{3-} - 4H^+ + 2Na^+]^{5-}$ at $m/z = 1129$ as the precursor ion. The overall tandem MS spectrum is shown in Fig. S12. Nearly all fragments below $m/z = 1000$ can be identified from their isotope patterns. These fragments are marked $1 - 10$ in Fig. S12. Since there is conservation of mass and charge during fragmentation, the m/z values of the corresponding fragments can be calculated and are all found in the spectrum (marked $1' - 10'$).

Detailed spectra of fragments $1 - 10$, along with theoretical spectra, can be found in Fig. S13. The tandem MS spectrum has very low intensity, so to ensure correct identification of these species we compared the ion signals with those obtained from MS with high sample cone voltage (SCV = -50 V).

When performing MS with SCV = -50 V, we also observed some Ag_7 and Ag_8 fragments which are not found in the tandem MS spectrum (Fig. S14). It is possible that these fragments are only formed at very high voltages, or that the intensity of these fragments is too low to observe in the tandem MS spectra (the abundance of Ag_7 and Ag_8 fragments in the high SCV spectrum is less than 10% of the most abundant fragments).

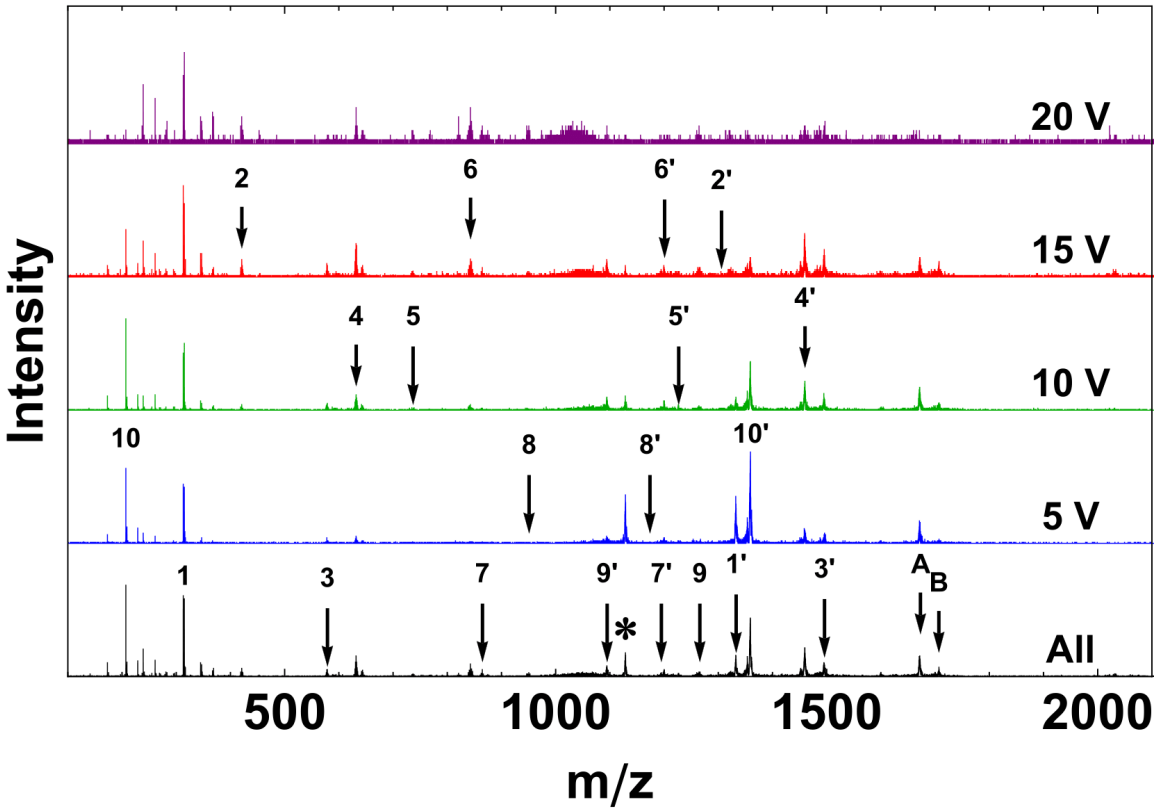

Figure S12 Tandem MS spectra of precursor $m/z = 1129$, at various collision voltages. The bottom spectrum shows the sum of all individual spectra. In total, 1650 spectra were recorded. The precursor is marked *. Small fragments are marked with numbers $1 - 10$, the corresponding larger fragments are marked $1' - 10'$. For example, fragment 4 was identified as $[Ag_6(LA)_3 - 2H^+]^{2-}$, which means the corresponding fragment $4'$ must be $[\{Ag_{23}(LA)_9\}^{3-} - 2H^+ + 2Na^+]^{3-}$ with mass 4381 Da and $m/z = 1460$. An ion signal corresponding to this fragment is clearly observed. The small fragments $1 - 10$ are shown in more detail and compared with theoretical spectra in Fig. S13. The fragments marked A and B result from multiple fragmentations and correspond to $[Ag_{27}(LA)_{10}]^{3-}$ and $[Ag_{28}(LA)_{10}]^{3-}$, respectively.

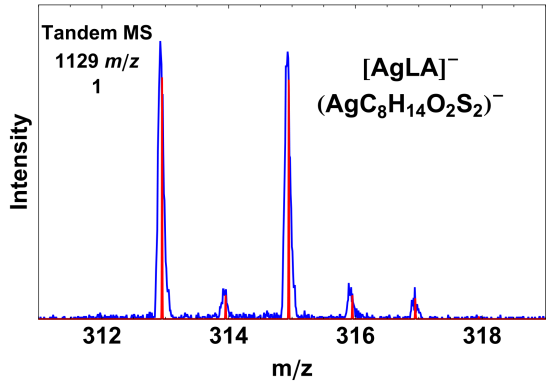
Tandem MS
1129 m/z
1
[AgLA]⁻
(AgC8H14O2S2)⁻
Intensity
312
314
316
318
m/z

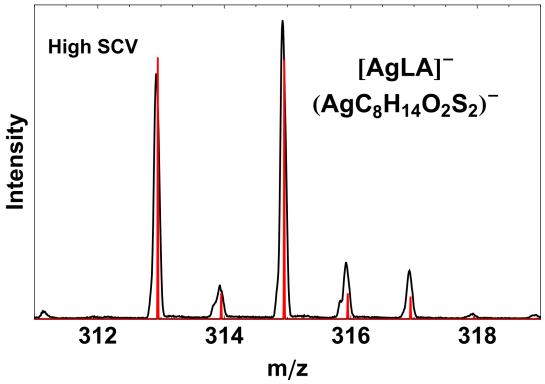
High SCV
[AgLA]⁻
(AgC8H14O2S2)⁻
Intensity
312
314
316
318
m/z

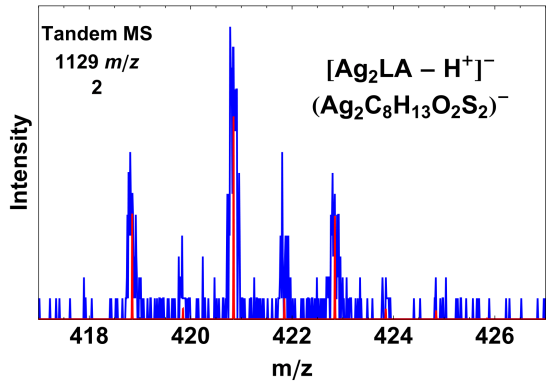
Tandem MS
1129 m/z
2
[Ag2LA – H+]⁻
(Ag2C8H13O2S2)⁻
Intensity
418
420
422
424
426
m/z

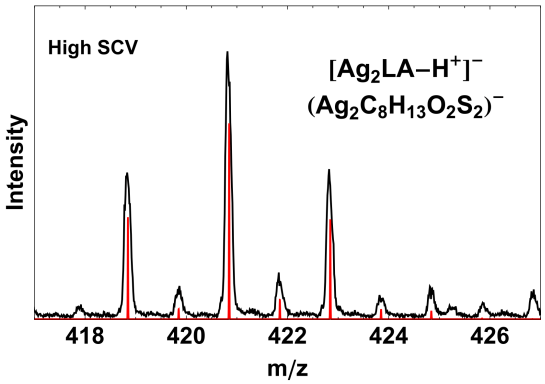
High SCV
[Ag2LA–H+]⁻
(Ag2C8H13O2S2)⁻
Intensity
418
420
422
424
426
m/z

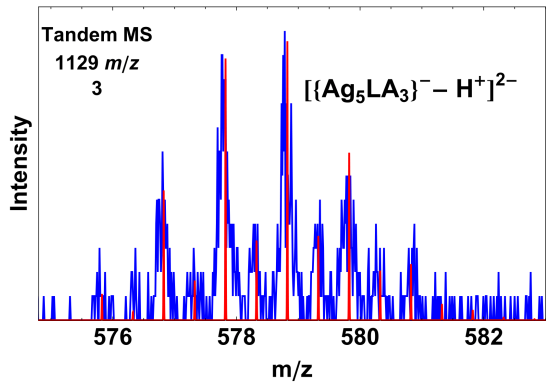
Tandem MS
1129 m/z
3
[{Ag5LA3}⁻– H+]2–
Intensity
576
578
580
582
m/z

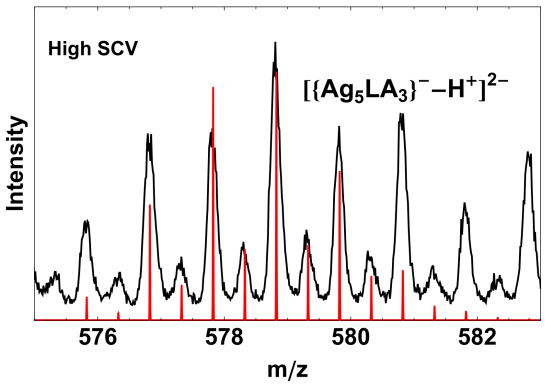
High SCV
[{Ag5LA3}⁻–H+]2–
Intensity
576
578
580
582
m/z

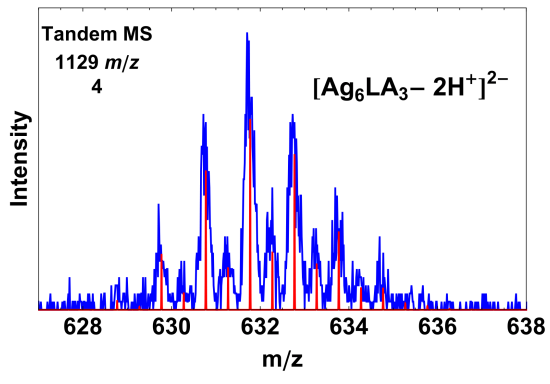
Tandem MS
1129 m/z
4
[Ag6LA3– 2H+]2–
Intensity
628
630
632
634
636
638
m/z

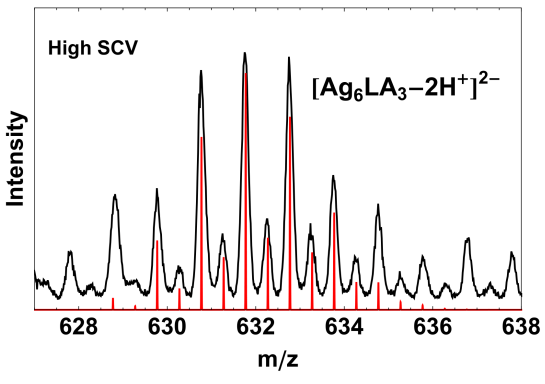
High SCV
[Ag6LA3–2H+]2–
Intensity
628
630
632
634
636
638
m/z

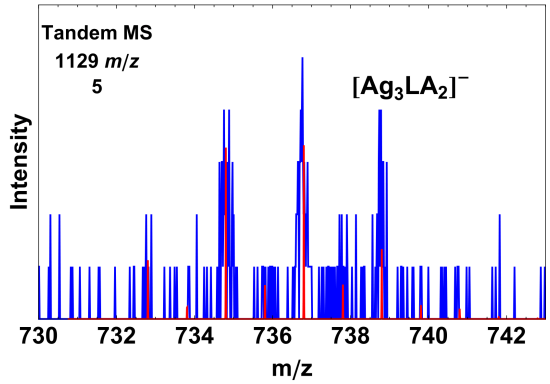
Tandem MS
1129 m/z
5
[Ag3LA2]−
Intensity
730 732 734 736 738 740 742
m/z

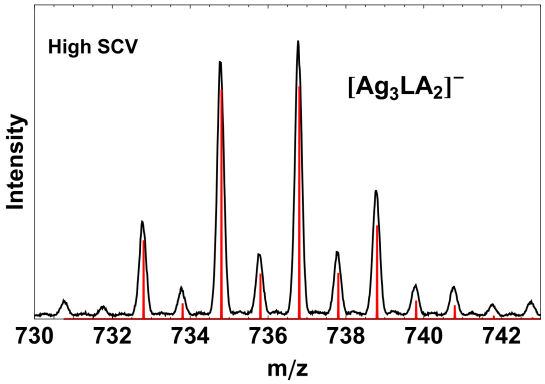
High SCV
[Ag3LA2]−
Intensity
730 732 734 736 738 740 742
m/z

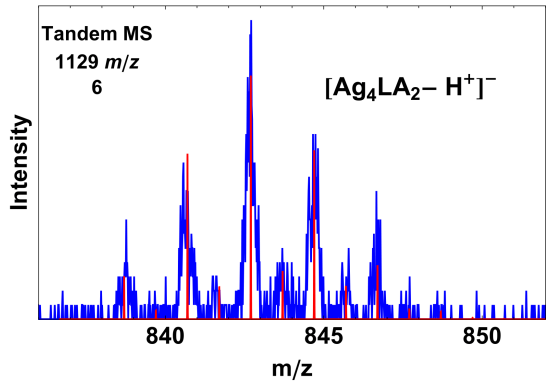
Tandem MS
1129 m/z
6
[Ag4LA2− H+]−
Intensity
840 845 850
m/z

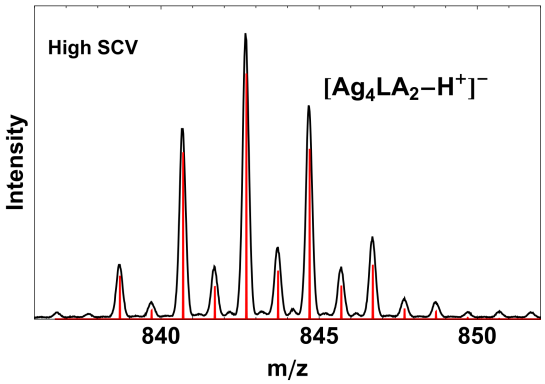
High SCV
[Ag4LA2−H+]−
Intensity
840 845 850
m/z

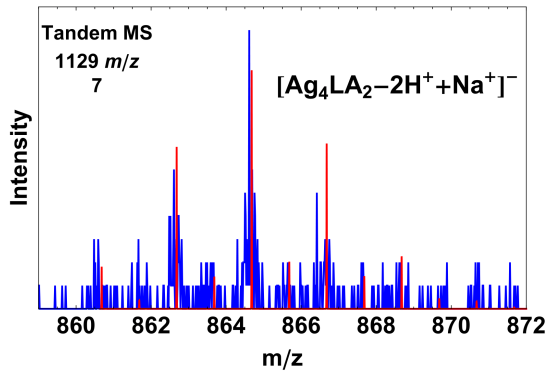
Tandem MS
1129 m/z
7
[Ag4LA2−2H++Na+]−
Intensity
860 862 864 866 868 870 872
m/z

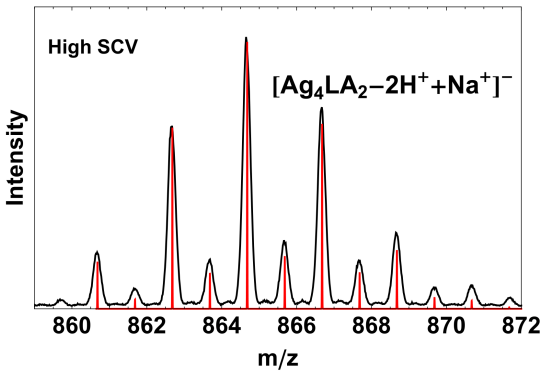
High SCV
[Ag4LA2−2H++Na+]−
Intensity
860 862 864 866 868 870 872
m/z

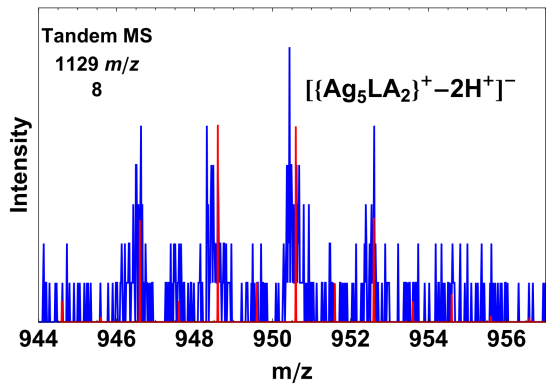
Tandem MS
1129 m/z
8
[{Ag5LA2}+−2H+]−
Intensity
944 946 948 950 952 954 956
m/z

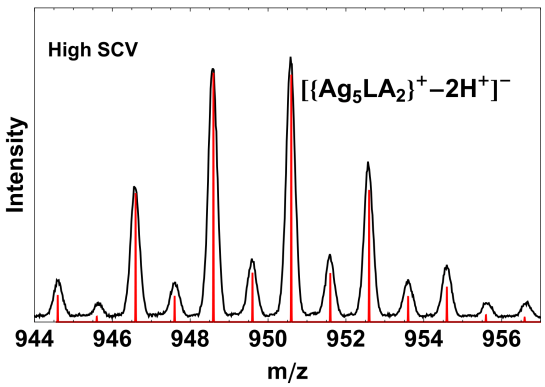
High SCV
[{Ag5LA2}+−2H+]−
Intensity
944 946 948 950 952 954 956
m/z

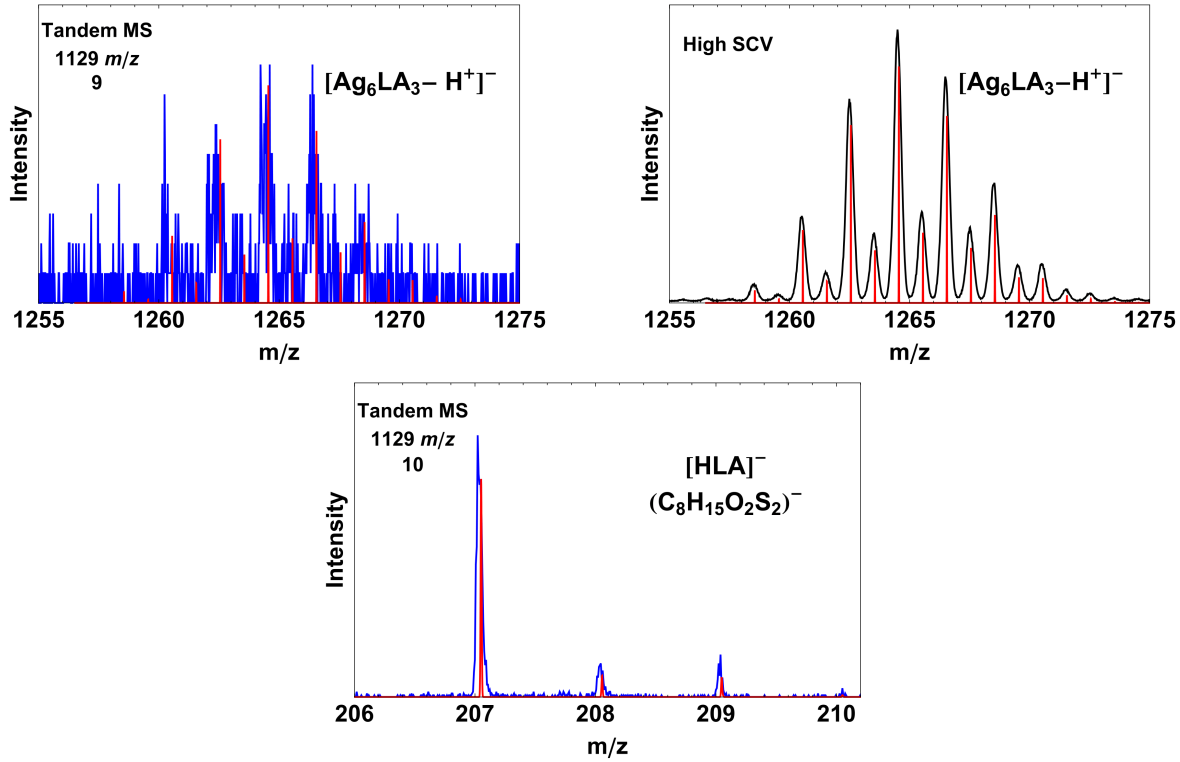

Figure S13 Cluster fragments observed during tandem MS of precursor $m/z = 1129$ (left, blue) and during MS with SCV = $-50\,\mathrm{V}$ (right, black). Theoretical isotope patterns are shown in red. The fragment $[\mathrm{HLA}]^-$ is not observed during MS with SCV = $-50\,\mathrm{V}$.

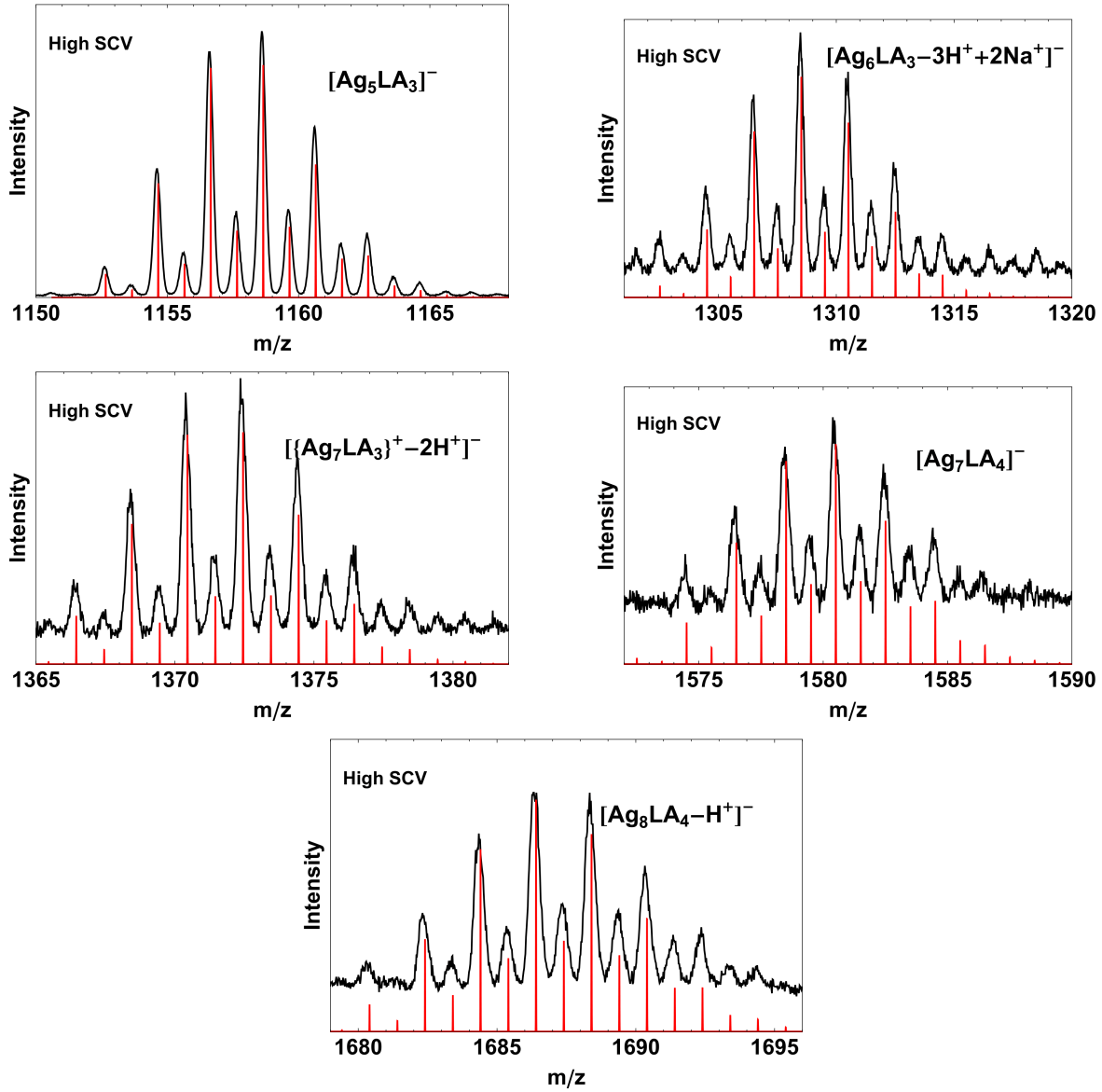

Figure S14 Cluster fragments observed during MS with SCV = $-50\,\mathrm{V}$ (black) and theoretical isotope patterns (red). These fragments are not observed during tandem MS of precursor $m/z = 1129$.

By raising the SCV to $-50\,\mathrm{V}$, we were able to select cluster fragments as precursors for tandem MS and investigate their fragmentation pathways. These have been briefly described in the main text. Spectra of precursor $m/z = 313 - 315$ ($[\mathrm{AgLA}]^-$) are given in Fig. S15 and S16, with detailed spectra of the fragments along with theoretical spectra in Fig. S17.

Figure S18 and S19 show tandem MS spectra of precursor $[\mathrm{Ag_6LA_3} - 2\mathrm{H}^+]^{2-}$ with $m/z = 632$ and $[\{\mathrm{Ag_5LA_3}\}^- - \mathrm{H}^+]^{2-}$ with $m/z = 580$, respectively.

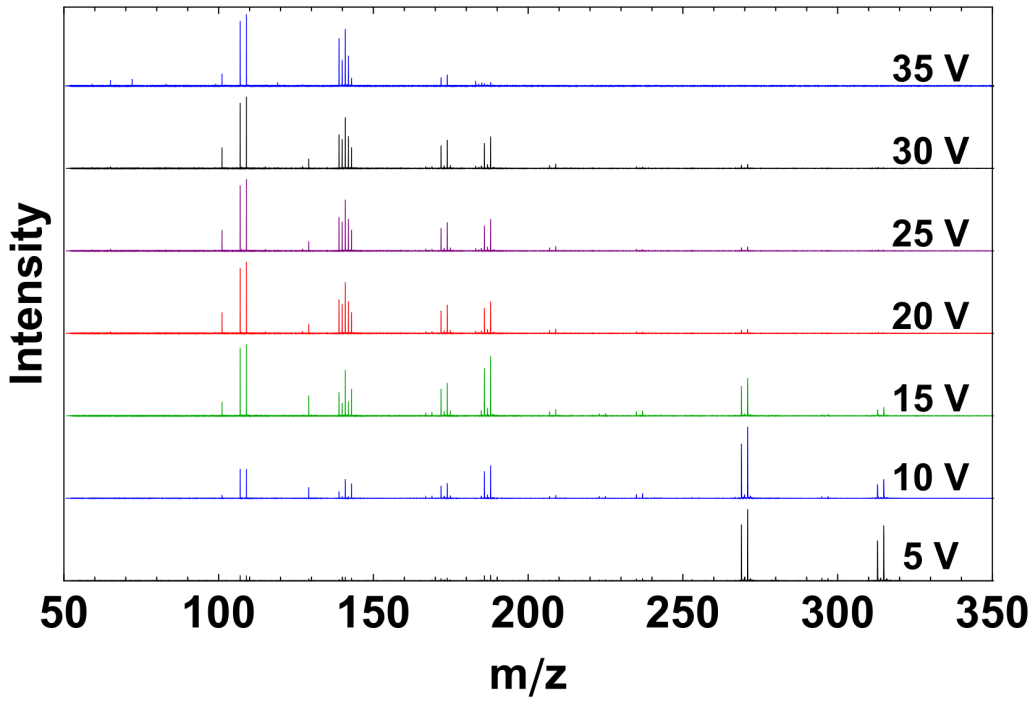

Figure S15 Tandem MS spectra of the precursor $[AgLA]^-$ for collision voltages of 5–35 V. The selection window for the precursor was broad enough to allow fragmentation of both $[^{107}AgLA]^-$ and $[^{109}AgLA]^-$. In total, 867 scans were done.

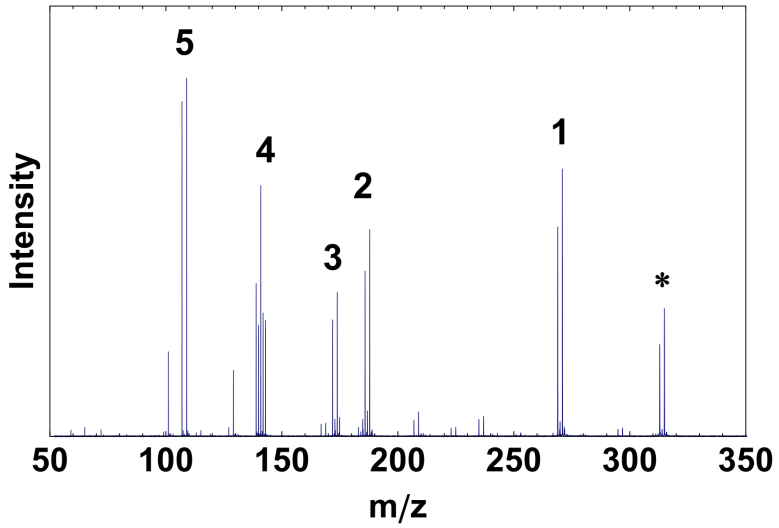

Figure S16 Sum of all tandem MS spectra of the precursor $[AgLA]^-$. The precursor is marked *, while fragments are marked $1-5$. Fragment 4 actually consists of three species, the ion signals of which overlap. Note that because the precursor has charge $z = 1-$, only one of the fragments of each fragmentation process is observed (the one carrying the charge).

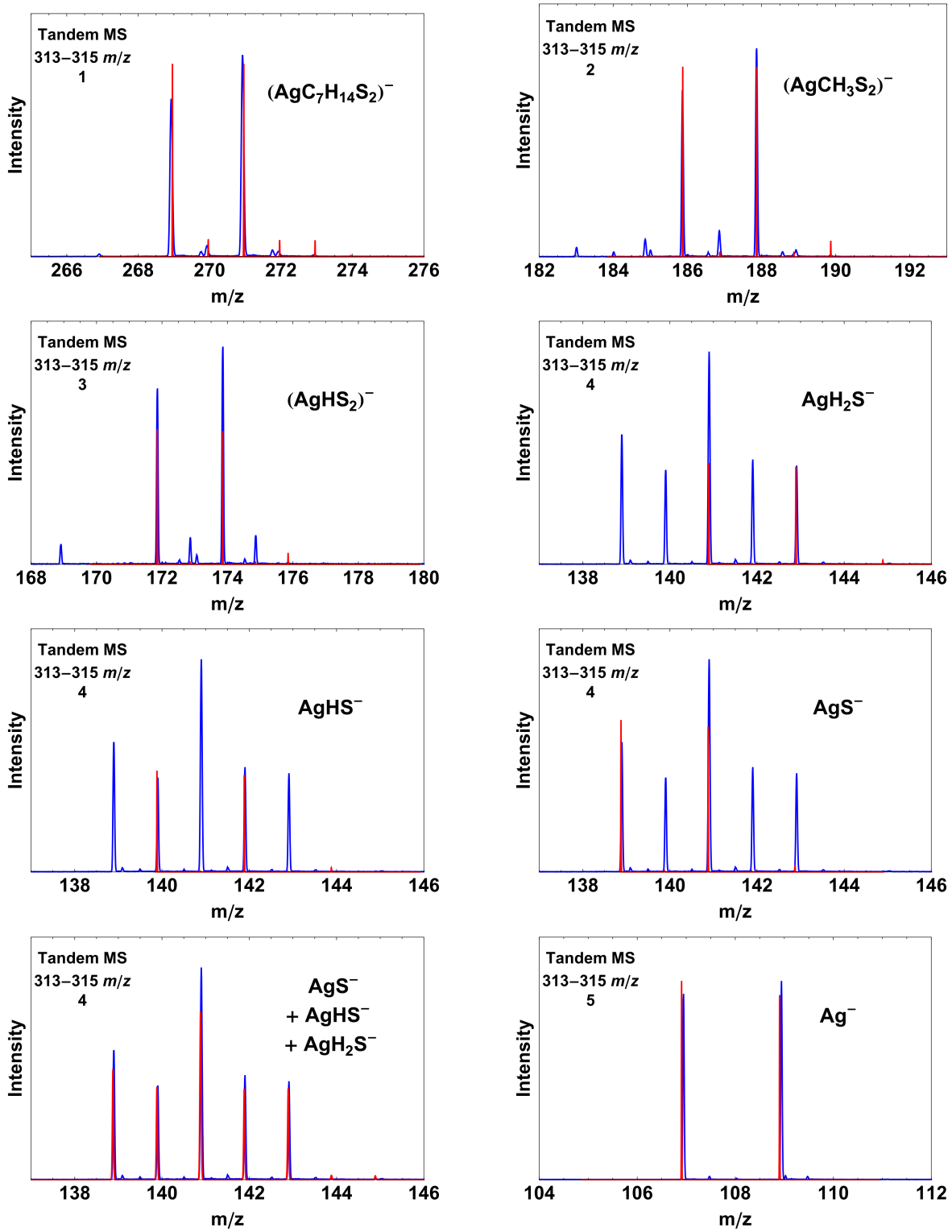

Figure S17 Fragments observed during tandem MS of precursor $[AgLA]^-$, $m/z = 313 - 315$ (blue). Theoretical isotope patterns are shown in red. For the theoretical spectrum of mixed species, the intensity of AgS^- was 1.2 times that of $AgHS^-$ and AgH_2S^-.

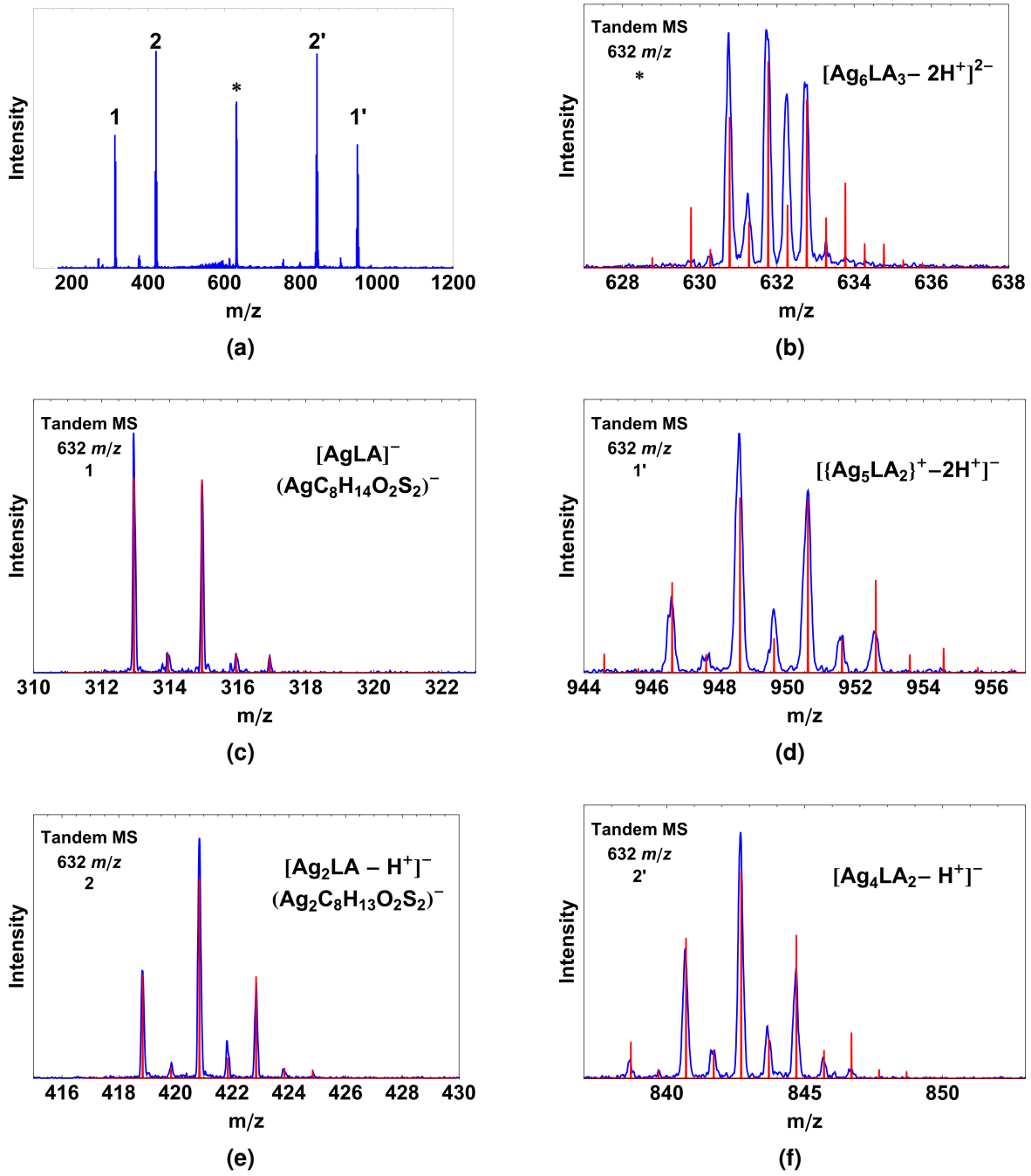

Figure S18 Tandem MS spectrum of the fragment $[Ag_6LA_3 - 2H^+]^{2-}$ with $m/z = 632$. Experimental data are shown in blue, theoretical isotope patterns in red. The precursor is marked with an * in figure (a) and its spectrum shown in more detail in figure (b). Figures (c-f) show the spectra of the fragments in more detail. The theoretical patterns are sometimes not an exact match for the experimental spectra, this is due to the narrow selection window for the precursor. All fragments are also observed in the tandem MS spectrum of the main cluster $m/z = 1129$.

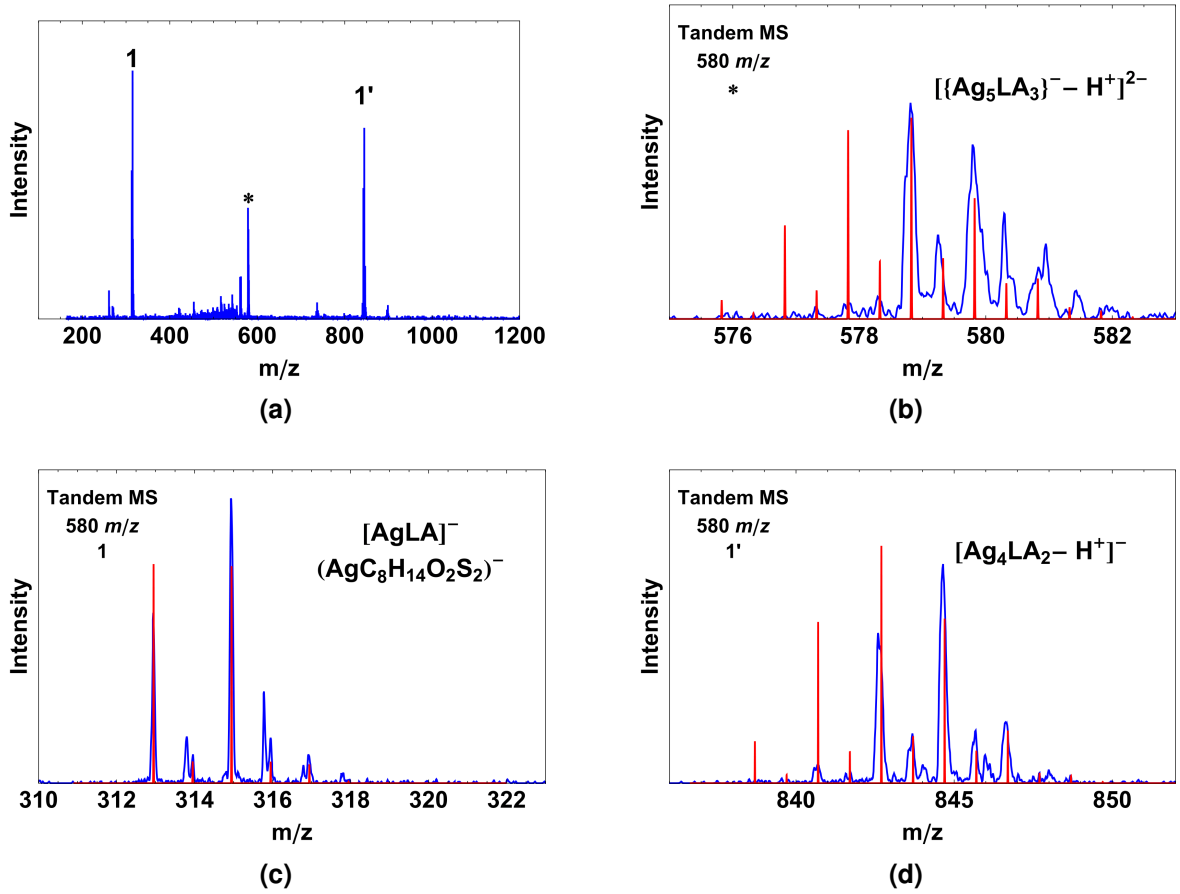

Figure S19 Tandem MS spectrum of the fragment $[\{(Ag_5LA_3)\}^- - H^+]^{2-}$ with $m/z = 580$. Experimental data are shown in blue, theoretical isotope patterns in red. The precursor is marked with an * in figure (a) and its spectrum shown in more detail in figure (b). Figures (c-d) show the spectra of the fragments in more detail. The theoretical patterns are sometimes not an exact match for the experimental spectra, this is due to the narrow selection window for the precursor. All fragments are also observed in the tandem MS spectrum of the main cluster $m/z = 1129$.

S4 Effect of purification on Ag cluster properties and stability

Absorption and emission spectra of clusters before and right after purification with BuOH are shown in Fig. S20.

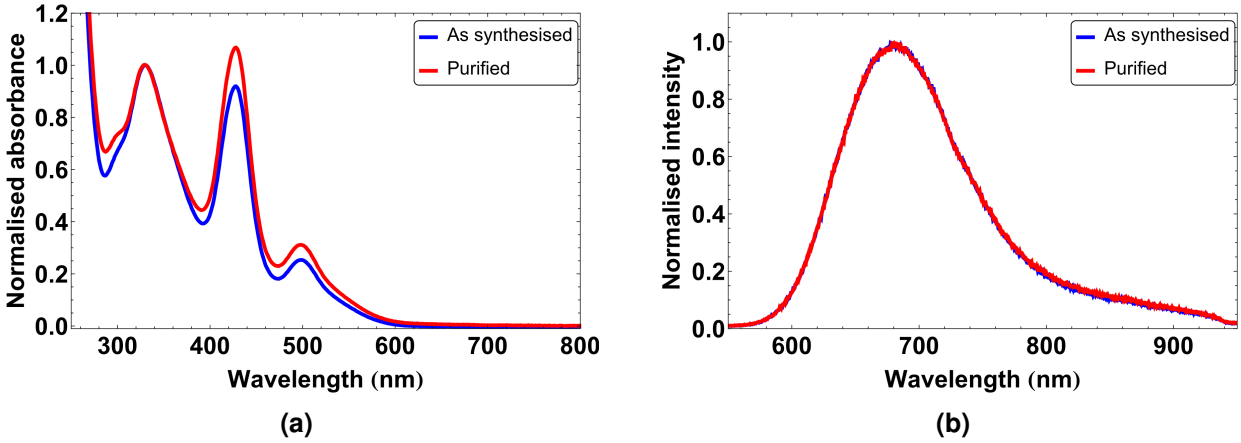

Figure S20 a) Normalised absorption and b) emission spectra of clusters before and after purification with BuOH. Spectra are normalised as the cluster concentration is not the same before and after purification. The emission from the purified clusters is bright and easily observable by eye. Emission spectra have not been corrected for spectral response as there is detector drift (ca 12 nm). The detector drift has been corrected. Absorption spectra are normalised at 330 nm.

UV-Vis absorption spectra of BuOH purified Ag clusters, at different times after purification, are presented in Fig. S21a and show a gradual disappearance of the pronounced absorption features. This coincides with a decrease in emission intensity (Fig. S22a), although the shape of the emission peak remains the same (S22b), indicating there is only one luminescent species.

Mass spectra recorded on the day of purification and a week later show changes in signal intensity for the Ag_{29} cluster (Fig. S23). The cluster signal increases at first but then it decreases and is barely discernible over the background after 1 week.

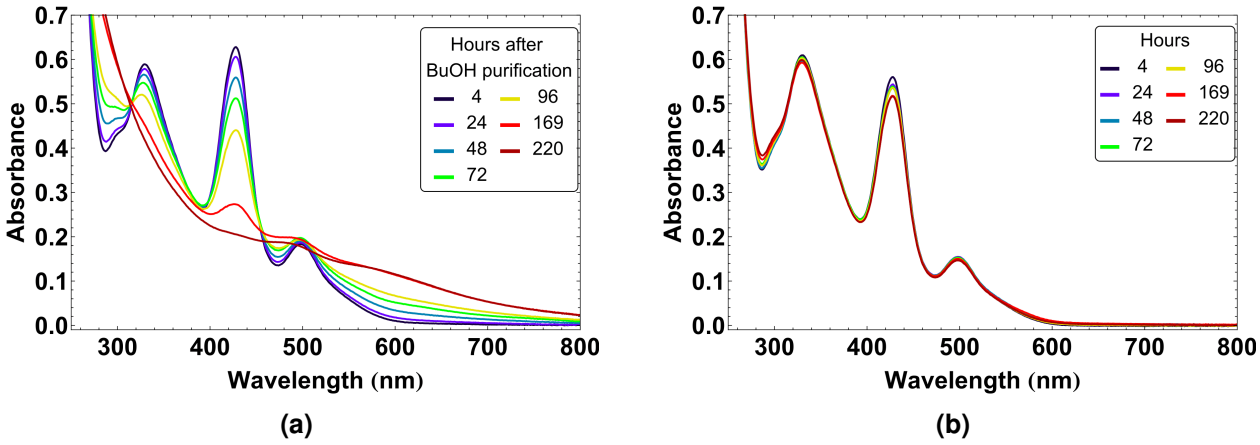

Figure S21 a) Absorption spectra of Ag clusters purified with BuOH at various times after purification. The pronounced absorption peaks gradually disappear and are gone after 220 hours (9 days). The as-synthesised clusters (b) hardly change during this time. Clusters are diluted 6x with water for the absorption measurement.

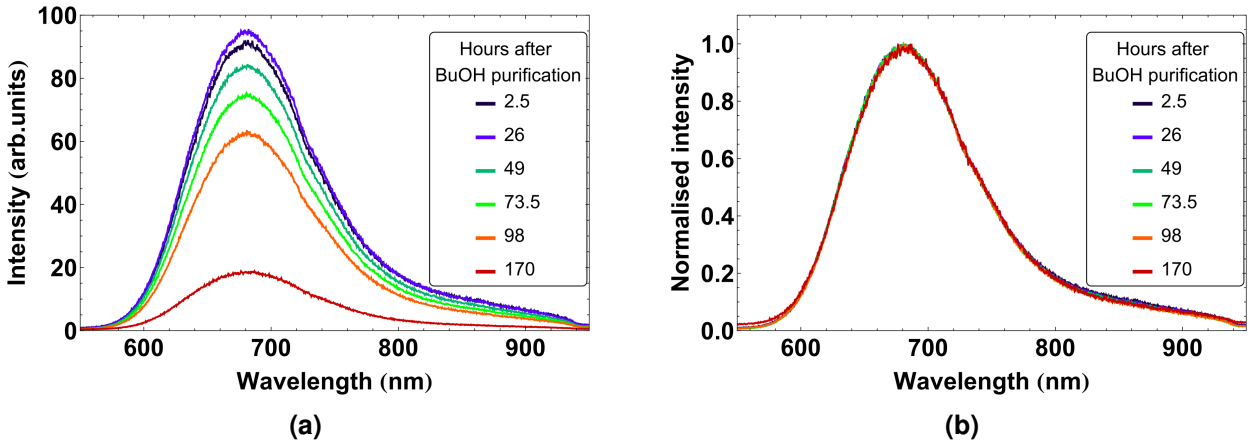

Figure S22 a) Emission spectra of Ag clusters purified with BuOH at various times after purification. The intensity gradually disappears, but the shape of the emission peak does not change (b), indicating a single luminescent species. Note that the emission spectra (a) have been divided by the maximum emission intensity of the as-synthesised sample measured on the same day. This was done because the emission intensity of as-synthesised spectra varied somewhat from day to day (this could be because the setup was inconsistent from day to day, and/or because the as-synthesised samples also change slightly during the week of measurements) The spectra have not been corrected for spectral response as there is detector drift (ca 12 nm) and this is not in the correction file. The detector drift has been corrected.

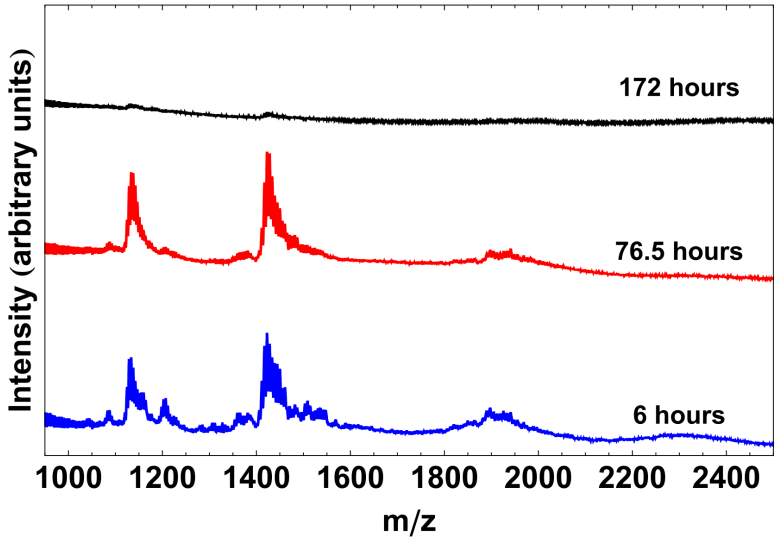

Figure S23 Mass spectra of Ag cluster sample at various times after BuOH purification, shifted vertically for clarity. The signal of the 5.6 kDa clusters ($m/z = 1120$ and 1400) is almost gone after 172 hours (1 week). Note that no new ion signals appear, i.e. the product of cluster degradation is not observed. Only three spectra are shown for clarity.

S5 Bleaching and regeneration

The as-synthesised Ag clusters remain stable for many months, although the characteristic optical properties disappear slowly over time (Fig. S24). Photobleaching with a 532 nm laser also causes cluster degradation (Fig. S26). The time-bleached (TB) and laser-bleached (LB) clusters have no strong absorption features (Fig. S27).

Transmission electron microscopy (TEM) images were recorded using a FEI Tecnai F30ST microscope in high-angle annular dark field (HAADF) mode operated at an accelaration voltage of 300 kV.

Sample purification was done with a 3 kDa cutoff filter. A drop of the purified solution was placed on a carbon coated copper (400-mesh) TEM grid.

Analysis of TB clusters with HAADF-TEM (Fig. S28) and AUC (Fig. 4) show that they are larger than the as-synthesised clusters.

Regeneration of TB and LB clusters with $NaBH_4$ gives samples with almost identical optical properties to fresh samples (Fig. S29). Regenerated clusters were characterised with SV-AUC and ESI-MS. The obtained distribution of sedimentation coefficients for regenerated clusters is shown in Fig. S30; it is identical to that of fresh clusters. Unfortunately, we were unable to purify the regenerated clusters with BuOH for ESI-MS. Once the last water had been extracted with BuOH and the clusters sedimented, they became brownish and could not be redispersed in water. Instead, we purified 500 µL regenerated clusters with 3 kDa filters. Filtration was done at 10.000 rpm, at room temperature. The clusters were washed 4x with water. The final concentrated, washed clusters solution (volume approximately 60 µL) was clear and orange. The mass spectrum (Fig. S31) shows a number of slightly lighter species in addition to the main $[Ag_{29}(LA)_{12}]^{3-}$ cluster (5.6 kDa). These species (identified in Fig. S32) could have been formed during the purification, as we know purification with filters causes some cluster degradation (Fig. S11).

TB clusters with low ligand concentration (Ag:LA = 1:0.6) can also be regenerated (Fig. S34). This is particularly successful if LA is added in addition to $NaBH_4$ (new ratio Ag:LA = 1:6.4, Figs. S33 and S35).

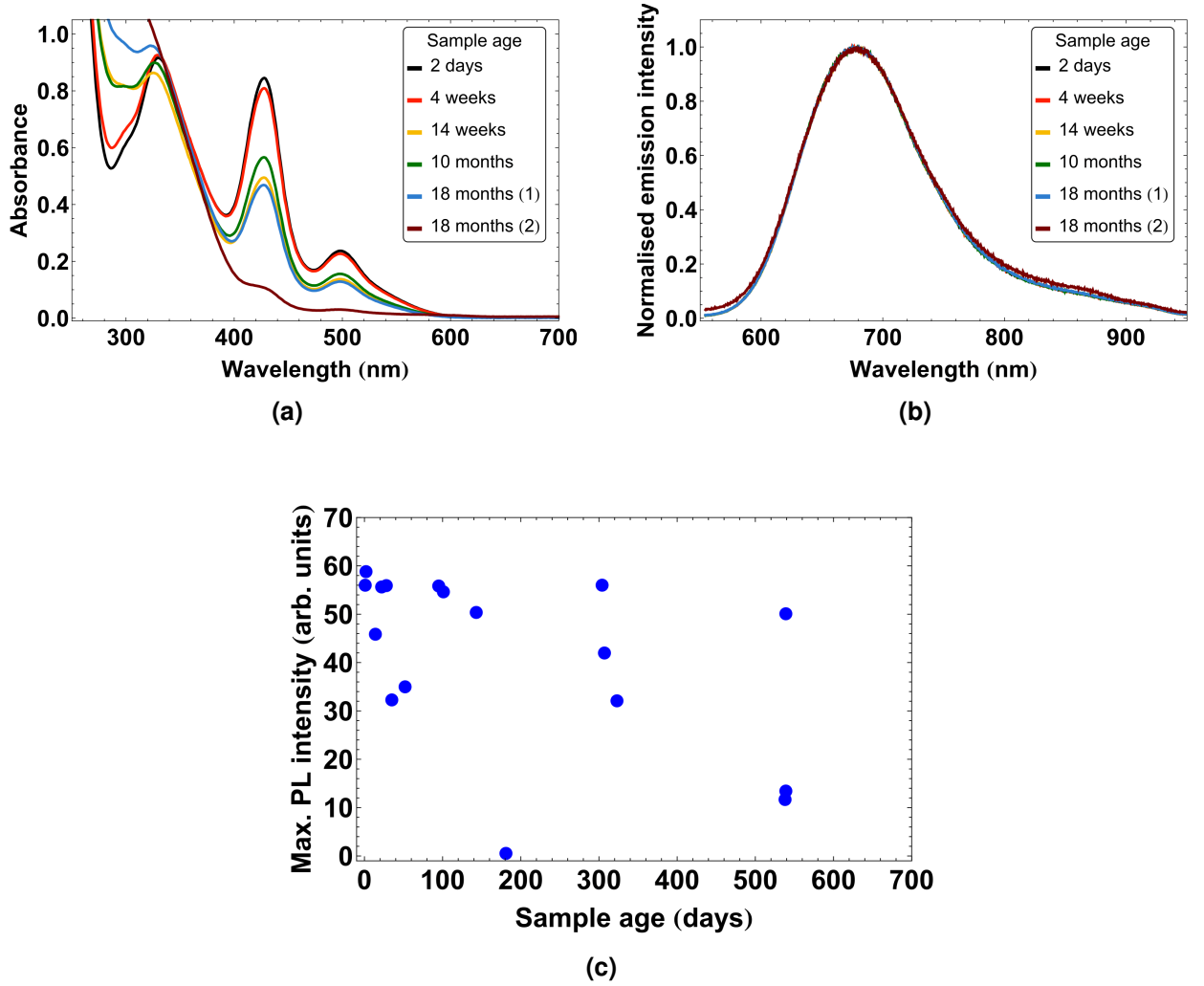

Figure S24 a) Absorption and b) normalised emission spectra of Ag clusters at various times after synthesis (during "time-bleaching"). c) Maximum emission (PL) intensity for samples at various times after the synthesis. The peaks in the absorption spectrum become less pronounced over time, and the emission intensity decreases. However, some samples are significantly more stable than others (note for example the large difference in absorption spectrum and emission intensity for the 18 month old samples). The shape of the emission peak does not change, indicating one luminescent species.

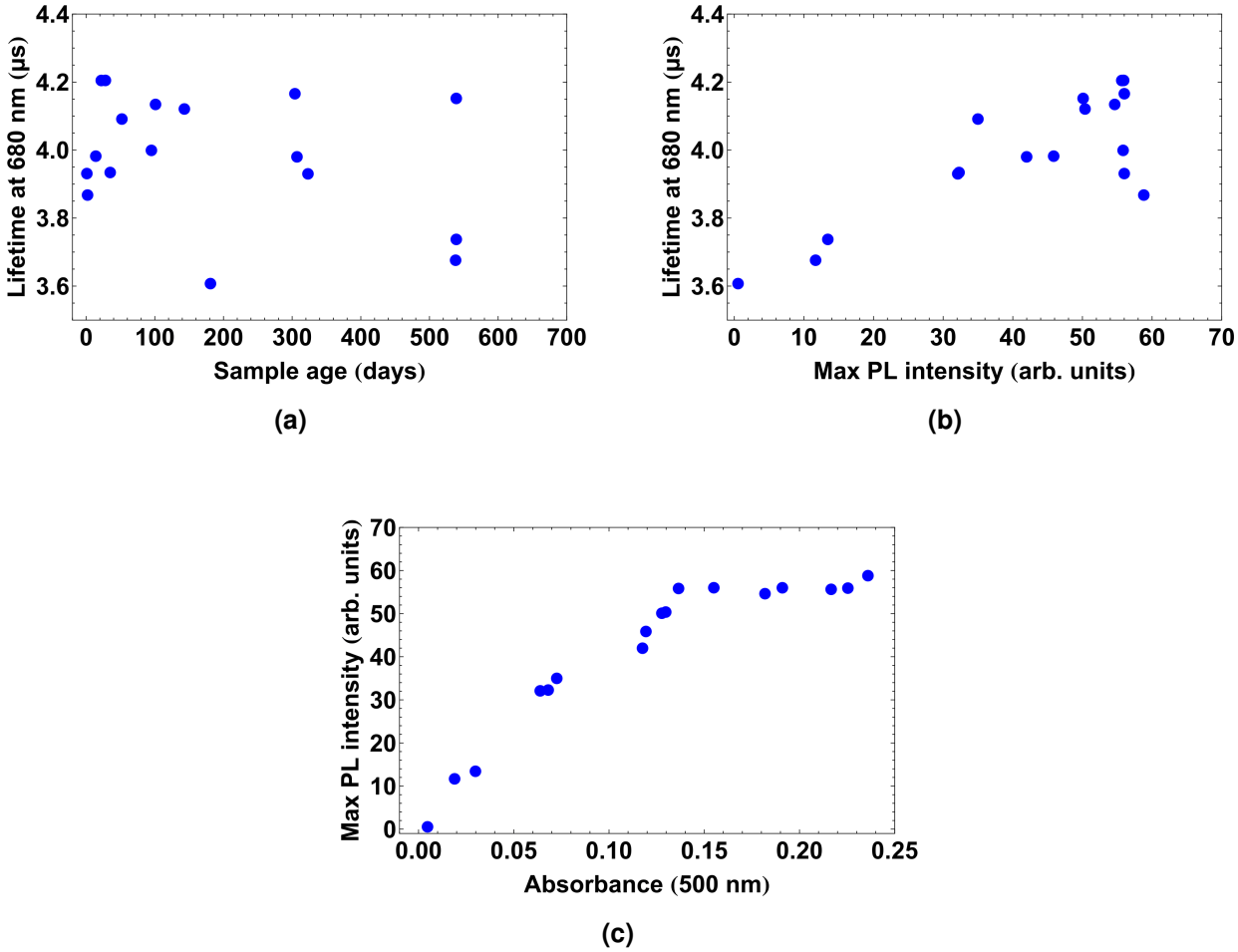

Figure S25 The dependence of the luminescence lifetime at $680\,\mathrm{nm}$ with a) sample age and b) maximum luminescence (PL) intensity. Since the extent of sample degradation does not only depend on sample age, but also exposure to light and air, the luminescence intensity or absorbance is a better measure for degradation than the time since synthesis. Also shown is c) the dependence of the luminescence intensity on absorbance. Below A$= 0.15$, there is linear behaviour while at higher absorbance quenching occurs.

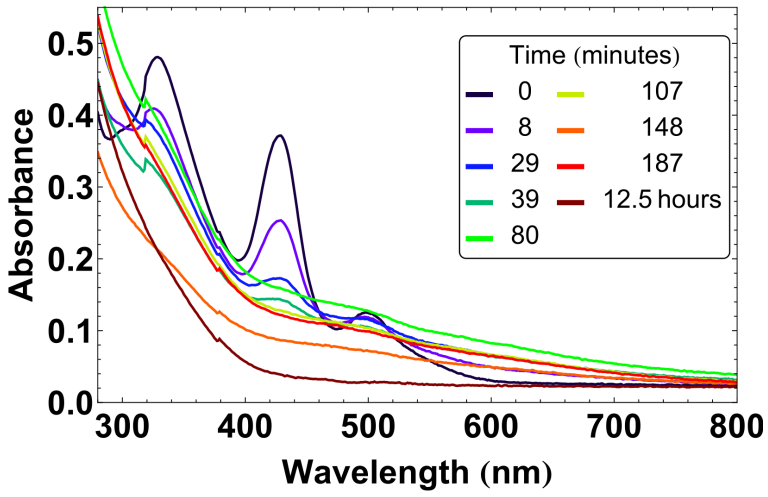

Figure S26 Absorption spectra of Ag clusters during photobleaching with a $532\,\mathrm{nm}$ laser. At t = 0 minutes, the laser is switched on.

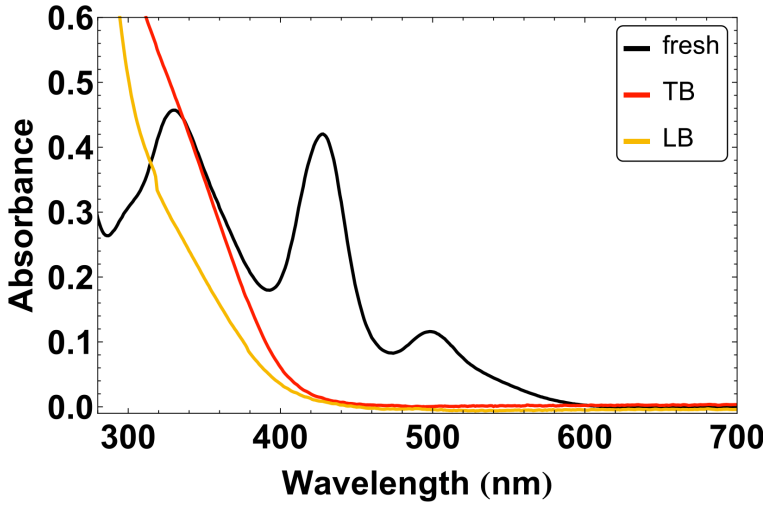

Figure S27 Absorption spectra of fresh, TB and LB clusters.

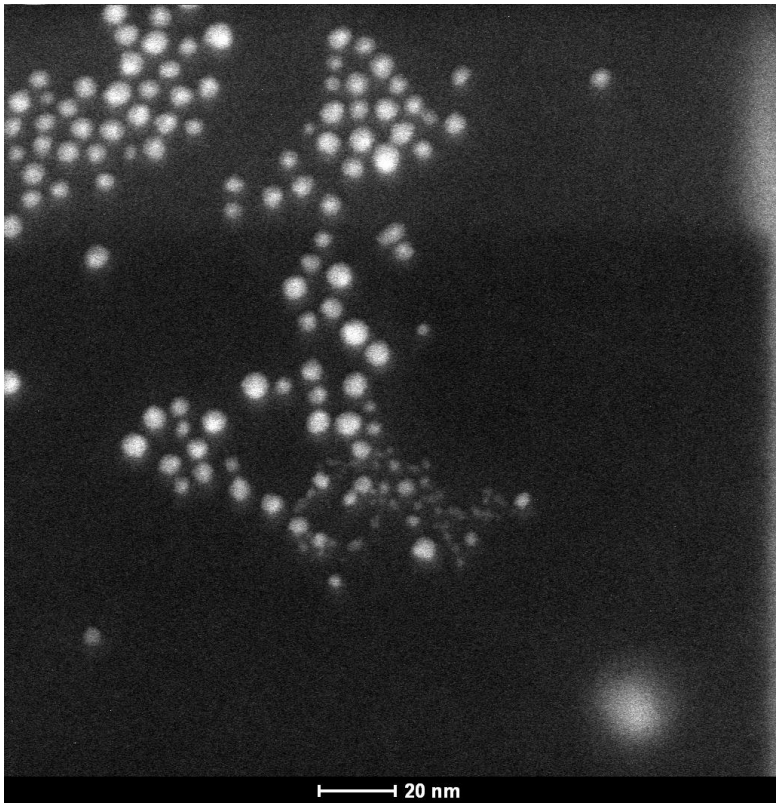

Figure S28 HAADF TEM image of TB clusters. Clearly large nanoparticles/aggregates are present. The scale bar is 20 nm.

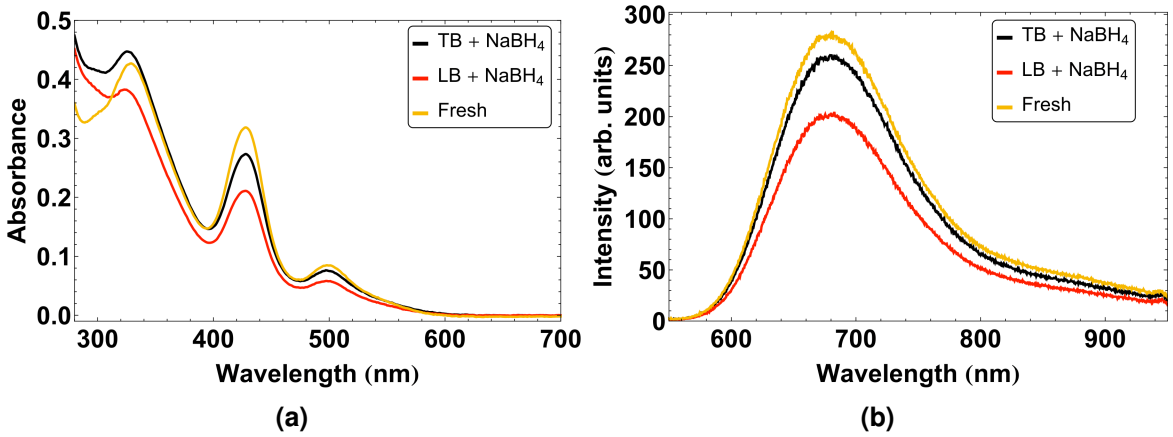

Figure S29 a) Absorption and b) emission spectra of regenerated TB and LB clusters. Spectra of fresh clusters are shown for comparison.

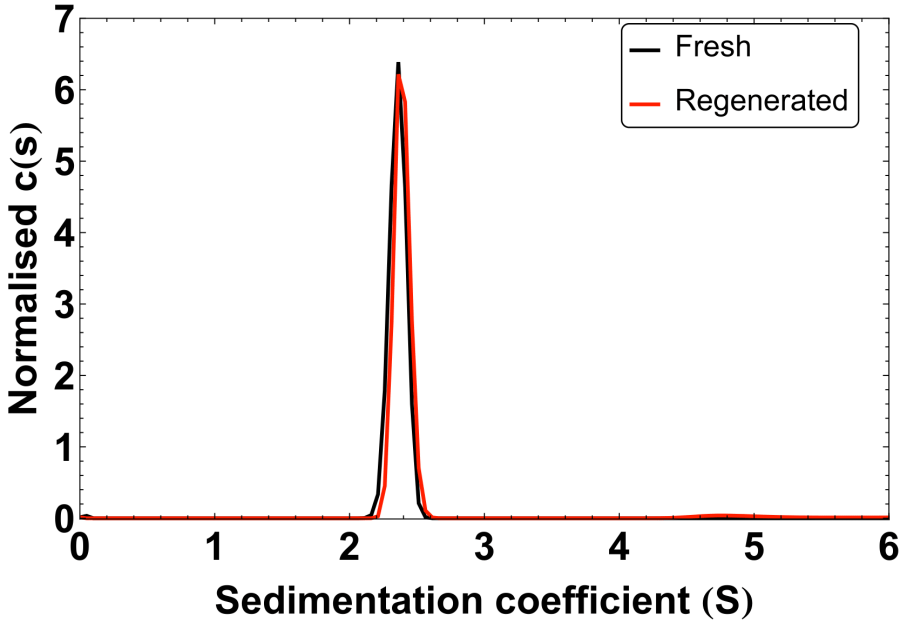

Figure S30 Distribution of sedimentation coefficients of fresh and regenerated clusters. Both samples were undiluted, and measured with absorption wavelength 528 nm and rotation speed 60.000 rpm.

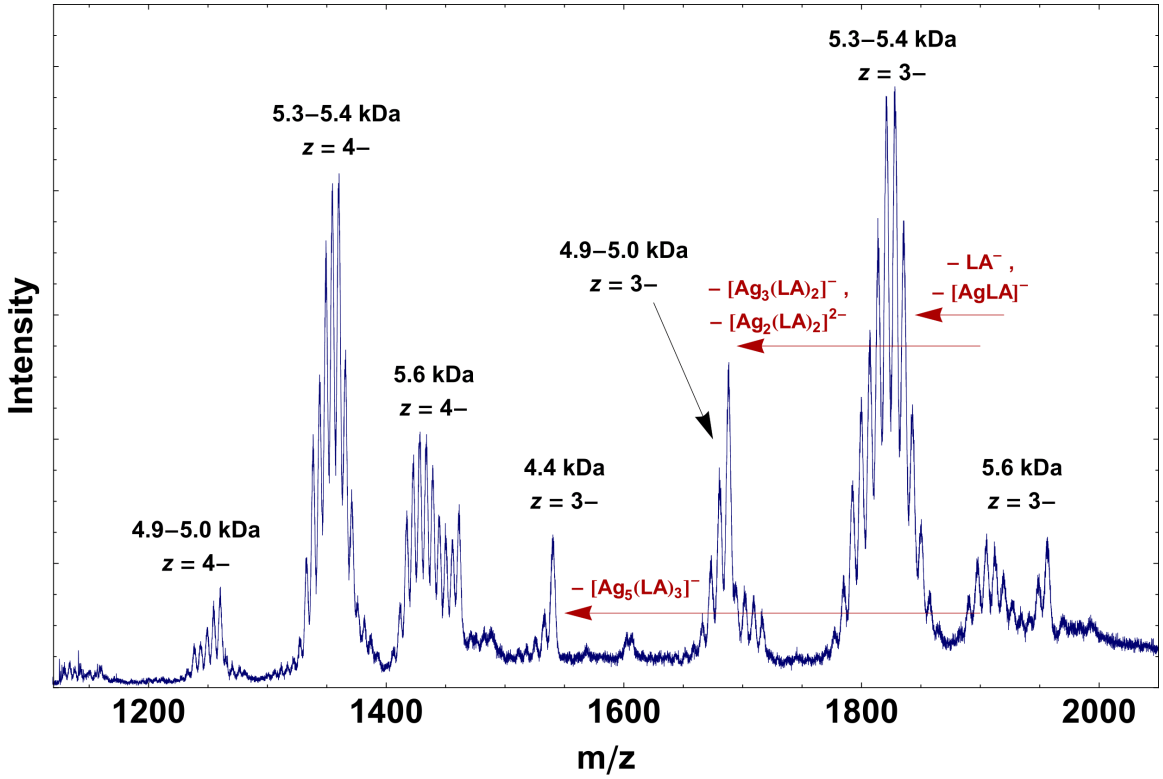

Figure S31 ESI-MS of regenerated clusters purified with $3\,\mathrm{kDa}$ filters. CV = $1100\,\mathrm{V}$ and SCV = $0\,\mathrm{V}$. The $[Ag_{29}(LA)_{12}]^{3-}$ clusters, mass $5.6\,\mathrm{kDa}$ are observed in $z = 4-$ and $3-$ overall charge states. A number of lighter species are also observed. Their masses and charges are indicated in the figure. The red arrows and text show how these lighter species can be formed from the Ag_{29} cluster (the species with $z = 4-$ are the same as those with $z = 3-$, but for clarity reasons arrows are only shown for $z = 3-$).

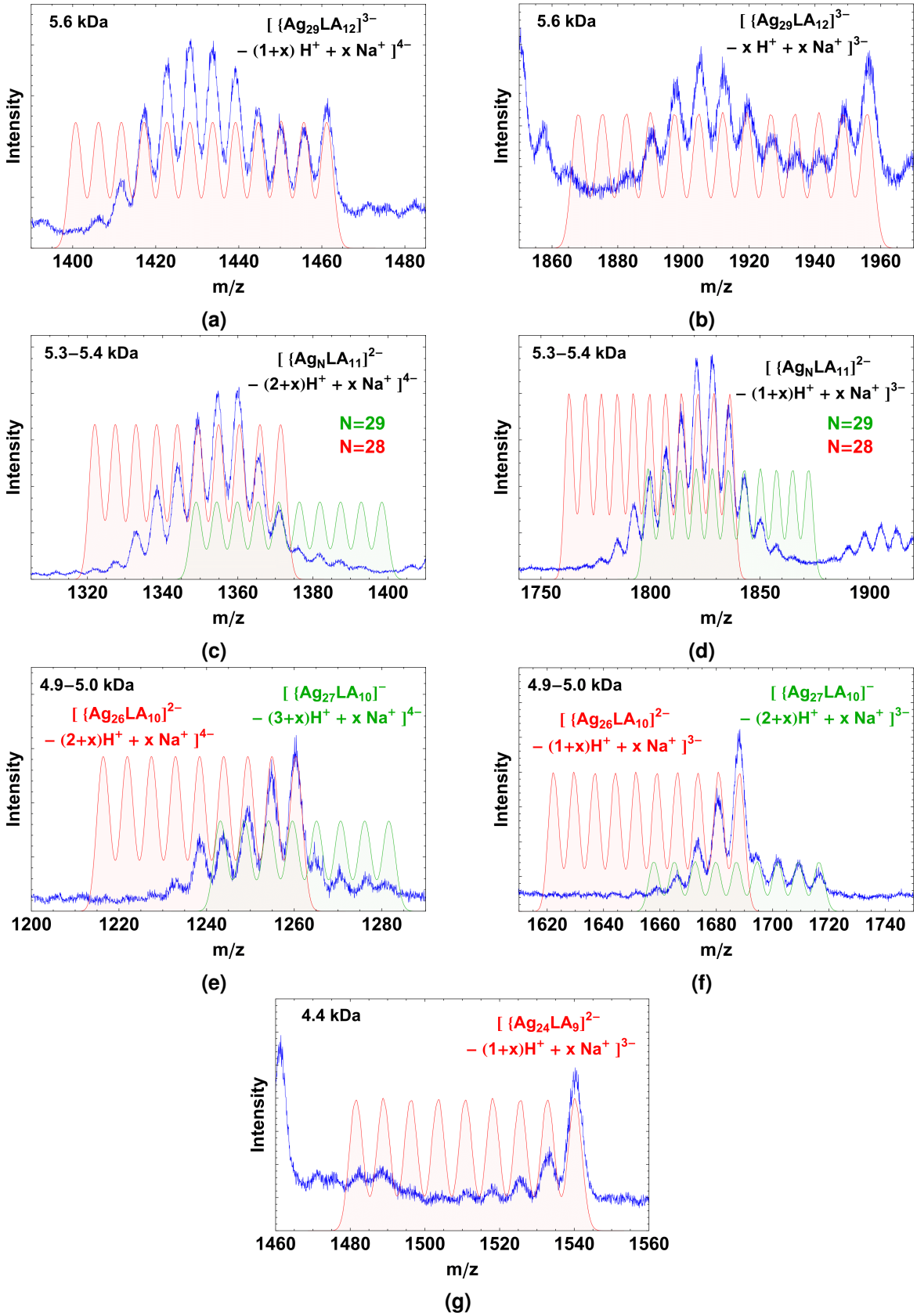

Figure S32 a) and b) show the 5.6 kDa species, $[Ag_{29}(LA)_{12}]^{3-}$, with theoretical spectra. c) and d) show the 5.3–5.4 kDa species, a combination of $[Ag_{29}(LA)_{11}]^{2-}$ and $[Ag_{28}(LA)_{11}]^{2-}$, with theoretical spectra. e) and f) show the 4.9–5.0 kDa species, a combination of $[Ag_{26}(LA)_{10}]^{2-}$ and $[Ag_{27}(LA)_{10}]^{-}$, with theoretical spectra. g) shows the 4.4 kDa species, $[Ag_{24}(LA)_{9}]^{2-}$, with theoretical spectrum.

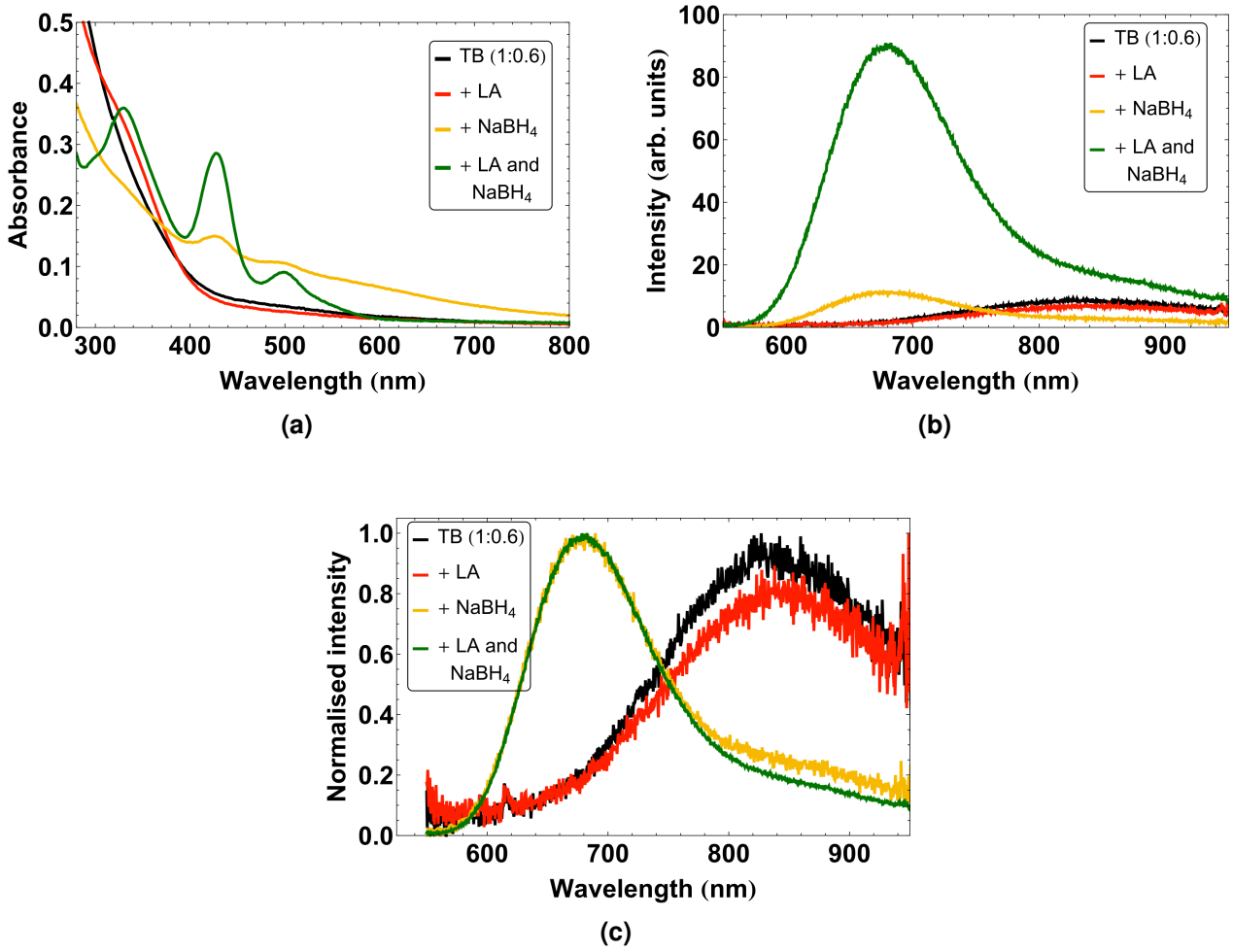

Figure S33 a) Absorption, b) emission and c) normalised emission spectra of TB clusters with Ag:LA = 1:0.6, and these clusters after regeneration with respectively LA, $NaBH_4$, and LA + $NaBH_4$. As can be seen, with the addition of just $NaBH_4$ there is some recovery of optical properties, but regeneration is more successful if also LA is added. The integration time of the CCD detector was 10x as long for TB and TB + LA as for the other two samples, as TB clusters have extremely low emission intensity

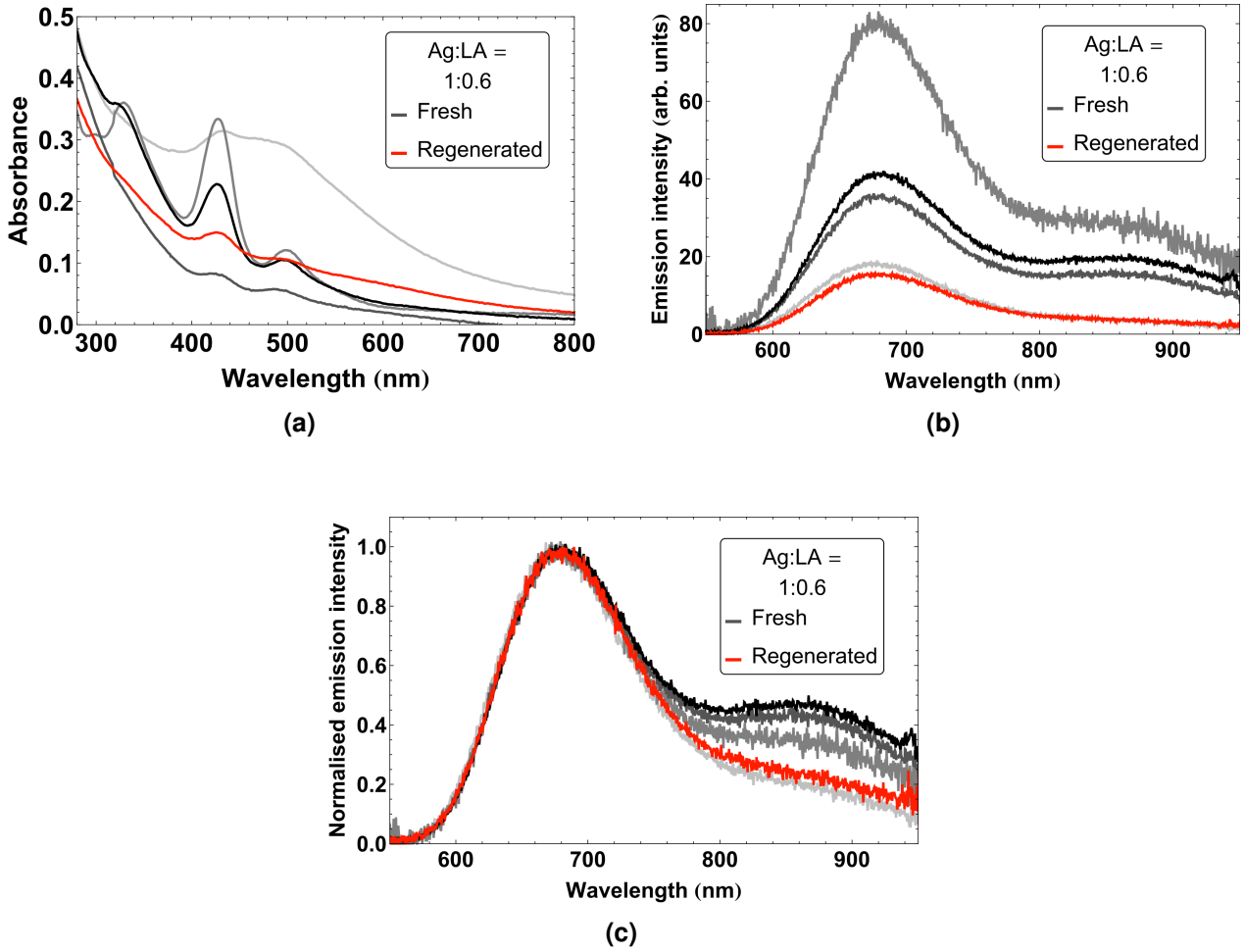

Figure S34 A comparison of optical properties of the regenerated TB Ag:LA = 1:0.6 samples (with just $NaBH_4$, red) with those of freshly prepared Ag:LA = 1:0.6 samples (grey and black). Absorption features are in reasonable agreement. The emission intensity of the regenerated sample is lower than that of freshly prepared samples but the shape of the emission peak is similar. Figures (a), (b) and (c) are absorption, emission and normalised emission spectra, respectively.

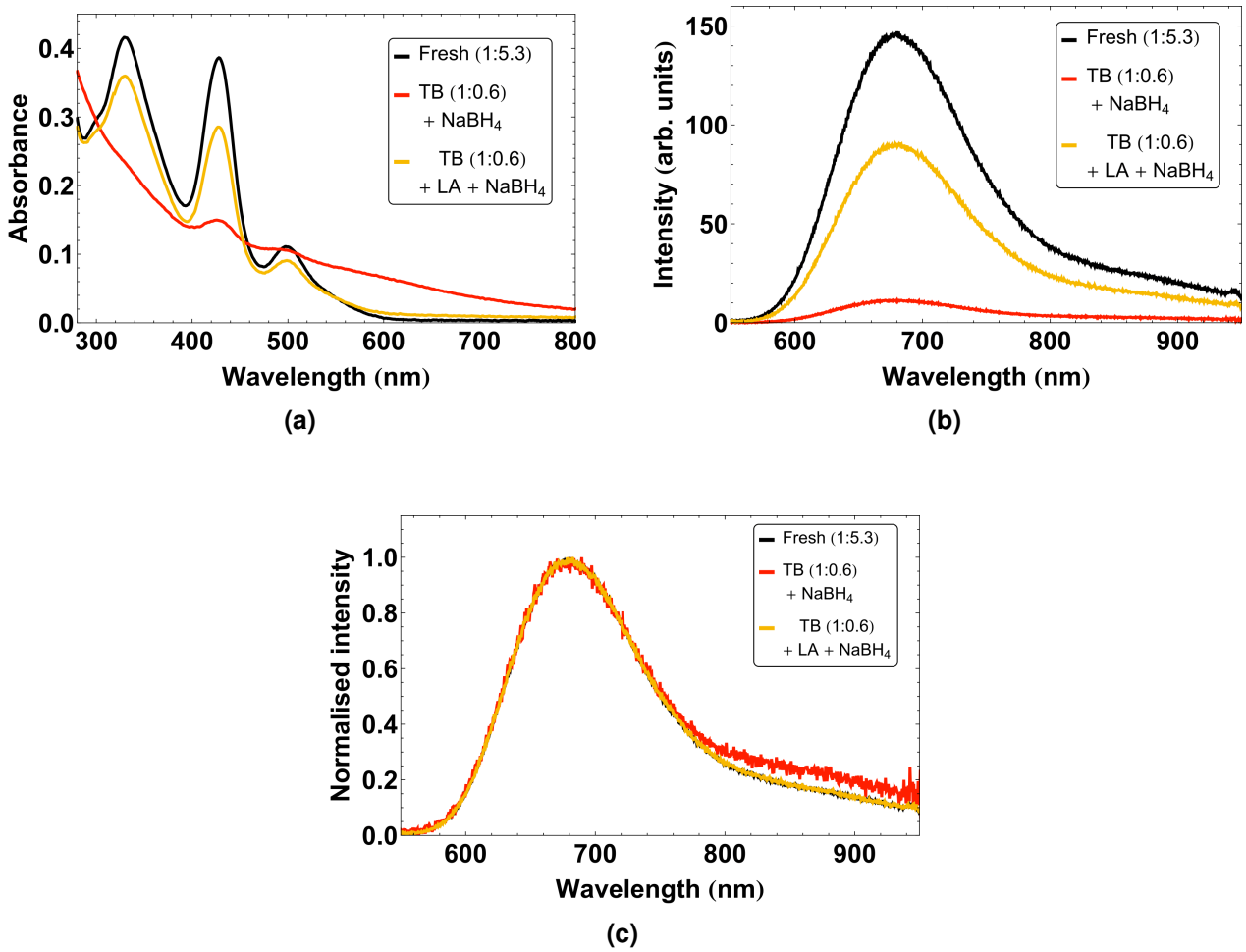

Figure S35 A comparison of optical properties of the two most successful regenerated TB Ag:LA = 1:0.6 samples (with just $NaBH_4$ and with LA + $NaBH_4$) with those of a freshly prepared Ag:LA = 1:5.3 sample (the standard Ag:LA ratio). The optical properties of a (LA + $NaBH_4$)-regenerated sample approach that of a fresh Ag:LA = 1:5.3 sample. Figures (a), (b) and (c) are absorption, emission and normalised emission spectra, respectively.

References

[1] I. Russier-Antoine, F. Bertorelle, R. Hamouda, D. Rayane, P. Dugourd, Z. Sanader, V. Bonačić-Koutecký, P.-F. Brevet and R. Antoine, *Nanoscale*, 2016, **8**, 2892–2898.

[2] P. T. K. Chin, M. van der Linden, E. J. van Harten, A. Barendregt, M. T. M. Rood, A. J. Koster, F. W. B. van Leeuwen, C. de Mello Donega, A. J. R. Heck and A. Meijerink, *Nanotechnology*, 2013, **24**, 075703.